

Review

Controlled Nickel Nanoparticles: A Review on How Parameters of Synthesis Can Modulate Their Features and Properties

Felipe Anchieta e Silva ¹, Vera Maria Martins Salim ²  and Thenner Silva Rodrigues ^{1,*} 

¹ Nanotechnology Engineering Program, Alberto Luiz Coimbra Institute for Graduate Studies and Research in Engineering, Federal University of Rio de Janeiro, Av. Horácio Macedo, 2030, Rio de Janeiro 21941-972, RJ, Brazil; felipe.anchieta@coppe.ufrj.br

² Chemical Engineering Program, Alberto Luiz Coimbra Institute for Graduate Studies and Research in Engineering, Federal University of Rio de Janeiro, Av. Horácio Macedo, 2030, Rio de Janeiro 21941-972, RJ, Brazil; vera@peq.coppe.ufrj.br

* Correspondence: thenner@pent.coppe.ufrj.br

Abstract: Nickel nanoparticles have wide-ranging applications in diverse fields, including electronics, catalysis, and biomedicine. The unique properties of these nanoparticles depend on their physical and chemical attributes. Consequently, there is a growing interest in understanding the performance relationships through a nuanced comprehension of their controlled synthesis. This review explores the advancements related to precisely defined nickel nanoparticles, with a specific focus on unraveling the connections between performance and their physical/chemical characteristics. The emphasis is on elucidating how manipulating synthetic parameters, such as precursor concentration, reductant agent properties, temperature, time, and the presence of stabilizing agents, can provide additional avenues for refining the performance in terms of size and morphology. Through the analysis of each variable, we illustrate the methodology for synthesizing well-controlled nickel nanoparticles, showcasing the ability to exert precision over their composition, size, and surface morphology.

Keywords: nickel nanoparticles; synthesis method; purification method; controlled synthesis



Citation: e Silva, F.A.; Salim, V.M.M.; Rodrigues, T.S. Controlled Nickel Nanoparticles: A Review on How Parameters of Synthesis Can Modulate Their Features and Properties. *AppliedChem* **2024**, *4*, 86–106. <https://doi.org/10.3390/appliedchem4010007>

Received: 29 December 2023

Revised: 18 February 2024

Accepted: 1 March 2024

Published: 13 March 2024



Copyright: © 2024 by the authors. Licensee MDPI, Basel, Switzerland. This article is an open access article distributed under the terms and conditions of the Creative Commons Attribution (CC BY) license (<https://creativecommons.org/licenses/by/4.0/>).

1. Introduction

Nickel (Ni), a versatile transition metal in the VIII B group, has long been revered for its exceptional properties and low cost compared to noble metals, spanning a multitude of applications. In its bulk metallic form, nickel exhibits robust mechanical strength, excellent corrosion resistance, and notable conductivity, making it indispensable in industries ranging from metallurgy to electronics. As advancements in materials science and nanotechnology burgeon, nickel nanoparticles have emerged as a focal point of research, unlocking unprecedented opportunities for tailored material design and innovative applications.

The unique size-dependent properties of nickel nanoparticles, coupled with their enhanced reactivity, surface area, high surface energy level, strong magnetism, and low melting point, hold promise for innovations in catalysis, medicine, and electronics [1,2]. This convergence of traditional nickel metal attributes and the novel characteristics of nickel nanoparticles marks an exciting frontier in materials science, offering a rich tapestry of possibilities for technological advancements and interdisciplinary exploration. For example, Zhu et al. have been exploring the potential of nickel nanoparticles with the morphology of nanorings as memory cells [3]. Alloys of copper and nickel at the nanoscale are being investigated for use in controlled magnetic hyperthermia applications [4] due to their bioactivity [5]. Additionally, nickel nanoparticles have been applied to electrode materials [6] in batteries [7] and solar cells [8].

The significant impact of nickel nanoparticles on various applications stems from their nanoscale dimensions. This transformative shift from macroscale to nanoscale, as illustrated in the schematic representation contrasting numerous nanoparticles with bulk

nickel in Figure 1A, leads to substantial alterations in its optical, magnetic, and electronic properties [9–11]. In the macro form, nickel exhibits limited surface atom incorporation within the total atom count (Figure 1B). The final atomic layer aligns at the frontier of the nickel macroparticle, with dotted circles denoting the absent atoms on the surface. Surface energy, defined by the sum of dangling bonds between atoms and missing atoms, is compensated by the surplus of atoms within the bulk particle. This surplus aids in balancing the surface energy originating from the deficient atoms on the surface and reduces the interatomic spacing between surface and interior atoms. Contrastingly, at the nanoscale (Figure 1C), the scarcity of interior atoms fails to counterbalance the increased surface energy caused by dangling bonds adequately. This deficiency prompts atom approximation within the nanoparticles and a reduction in lattice parameters, consequently altering geometric and electronic structures [11–14]. Modification of these parameters can, in turn, lead to enhanced nanoparticle properties.

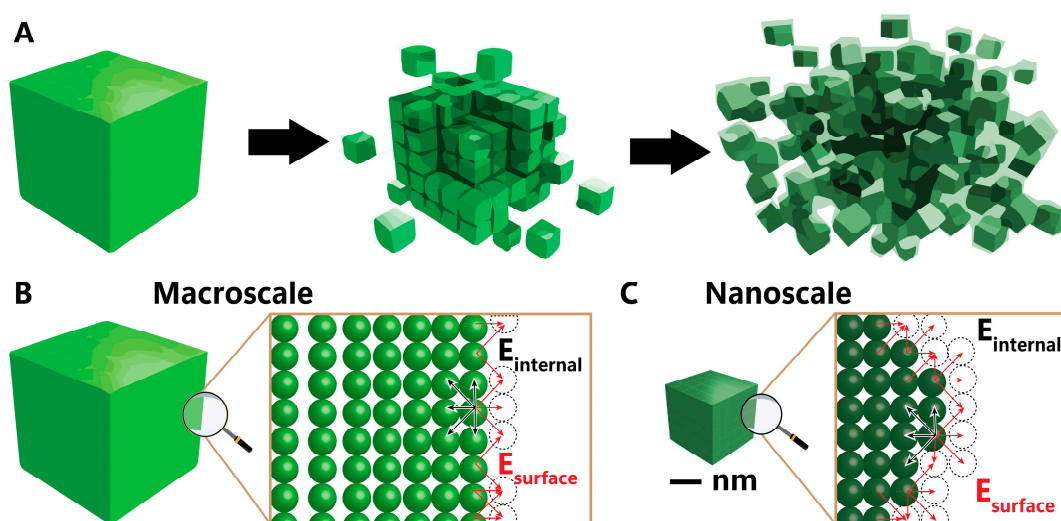


Figure 1. (A) Reduction scale from bulk to nano, (B) surface of bulk material, and (C) surface of nanomaterial. Black and red arrows indicate the internal and surface energies, respectively.

In this context, the properties of nanoparticles—such as size, shape, and structure—are intricately linked [15]. The crucial aspect in achieving monodisperse and uniform nanoparticles lies in effectively segregating the nucleation and growth processes. The LaMer plot elucidates the nanoparticle formation phenomenon (Figure 2), encompassing three distinct stages: (i) generation of atoms, (ii) nucleation, and (iii) growth [16–19].

During Stage I, metal ions undergo reduction to generate metallic atoms, serving as growth species (building blocks) for nucleus and nanoparticle formation. In this initial stage, the atoms lack sufficient energy for nucleus formation due to lower concentration. Once the concentration of atoms reaches the threshold necessary to overcome the energy barrier for homogeneous nucleation (Equation (1)), the formation of the nucleus ensues [16]. This critical point, marked by the red dot in the LaMer plot, signifies the attainment of the minimum concentration of metal atoms in solution, enabling their aggregation into a stable nucleus with a critical radius (r), surface free energy per unit area (γ), and free Gibbs energy (ΔG_v).

Stage II, the nucleation phase, involves the aggregation of atoms to shape the nucleus. This phase must occur rapidly in controlled synthesis to ensure uniform nucleus size. Conversely, an extended duration in this stage leads to varied nucleus sizes and a broad particle size distribution due to nucleus aggregation. Stage III, the growth phase, entails the aggregation of atoms on the surface of the nucleus to foster growth and nanoparticle

formation. Similar to the nucleation strategy, rapid growth is essential for achieving a narrow particle size distribution.

$$\Delta G = 4\pi r^2 \gamma + \frac{4}{3}\pi r^3 \Delta G_v \quad (1)$$

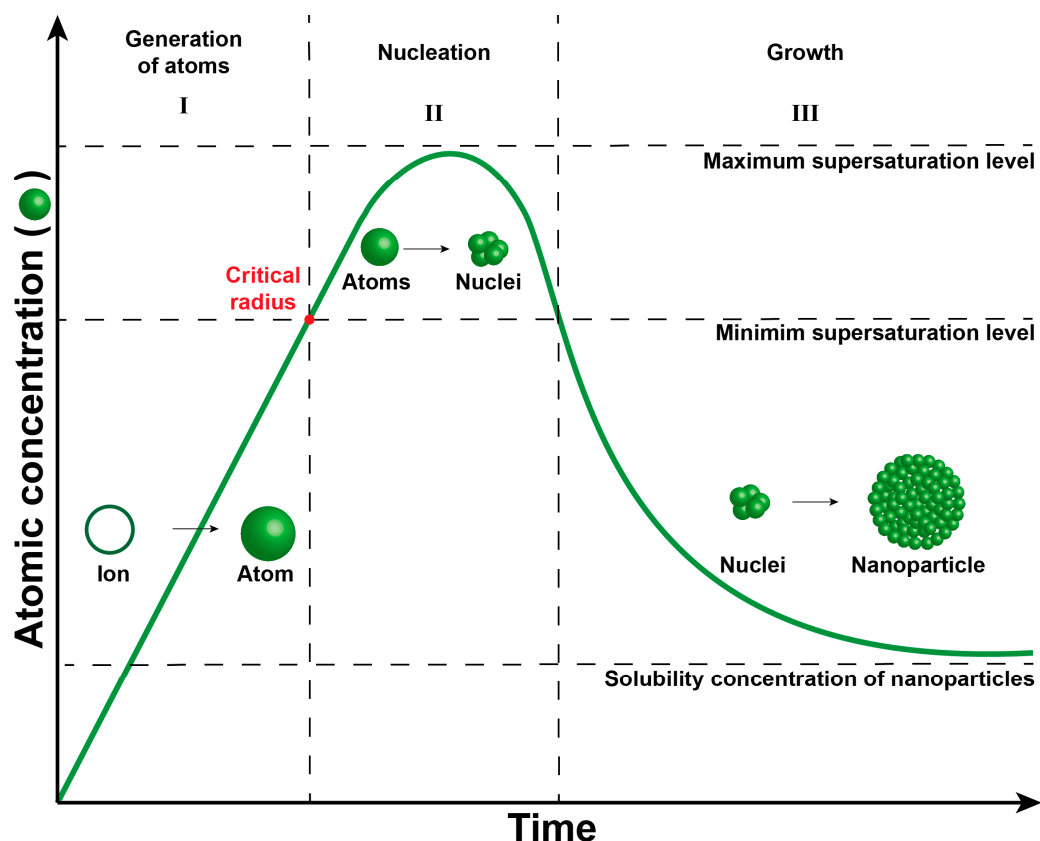


Figure 2. LaMer plot describing three stages of metal nanoparticle formation in the solution system. Stage I: Generation of atoms, stage II: Nucleation, and stage III: Growth.

The synthesis of nickel nanoparticles can be achieved through diverse methodologies depicted in the literature, including template-assisted, chemical reduction, and polyol methods, with possible assistance from intensification techniques such as microwaves and hydrothermal processes. Each methodology and the chosen operational conditions can influence distinct reaction mechanisms in the nucleation and growth steps, leading to variations in the morphological, size, and structural aspects of the nanoparticles [17]. Moreover, precise control over the nucleation and growth steps, and consequently over the size, morphology, and structure of the nanoparticles, can be attained by manipulating the operational conditions of the synthesis methodology. Factors such as the concentration and nature of the precursor, reducing agent, stabilizing agent, solvent, reaction temperature, and time play crucial roles in achieving this control [18]. For instance, the choice of solvent can impact ion diffusion, thereby modifying the size and shape of the nanoparticles. Some solvents, like ethylene glycol, can serve multiple functions, acting as both a stabilizing and reducing agent. Additionally, stabilizing, surfactant, and capping agents influence the morphology, size, and structure of the nanoparticles. During nucleation and growth, protective agents fixate on specific crystal faces to inhibit growth in that direction and prioritize other crystal faces. The reduction agent, dependent on its reduction potential, can control nucleation and growth rates, exerting a significant influence on the final nanoparticles. The reaction temperature affects solvent viscosity, impacting the diffusion of ions, nuclei, and particles [19]. In summary, this review focuses on discussing the parameters

such as precursor, reduction agent, stabilizing agent, solvent, and reaction temperature, and their influence on the morphological, size, and structural aspects of nickel nanoparticle synthesis, aiming to achieve well-controlled properties.

2. Nickel Nanoparticle Synthesis

The nickel salt is an important parameter because the counterion determines the solubility of the salt in the solvent and influences electrostatic stabilization, the pH modifier, and the complexing agent. Nickel nanoparticles can be synthesized through a variety of nickel salts, such as nickel (II) acetate ($\text{Ni}(\text{CH}_3\text{CO}_2)_2$) [20,21], nickel (II) bis(acetylacetonate) ($\text{Ni}(\text{C}_5\text{H}_7\text{O}_2)_2$) [22,23], nickel (II) nitrate ($\text{Ni}(\text{NO}_3)_2$) [24,25], nickel (II) oxalate (NiC_2O_4) [26], nickel chloride (NiCl_2) [27,28], nickel (II) sulfate (NiSO_4) [29], and nickel (II) dodecyl sulfate ($\text{Ni}(\text{DS})_2$) [30].

The concentration of nickel salt is a critical point that influences nucleation and growth ratio due to the chemical kinetic theory [31]. The precursor concentration is determinant to controlling the size and morphology and can be manipulated to promote complex morphologies, such as nanoflowers, spiky nanospheres, and spiky nanowires, and increases the nanoparticle size [32–34]. Figure 3 shows the influence of precursor concentration on the chain-like nanostructured materials; it is possible to see in these chain-like nanostructured materials that the diameters are 70 nm, 100 nm, 180 nm, and 380 nm for Ni^{2+} concentrations of 5 mM, 10 mM, 20 mM, and 50 mM, respectively [33].

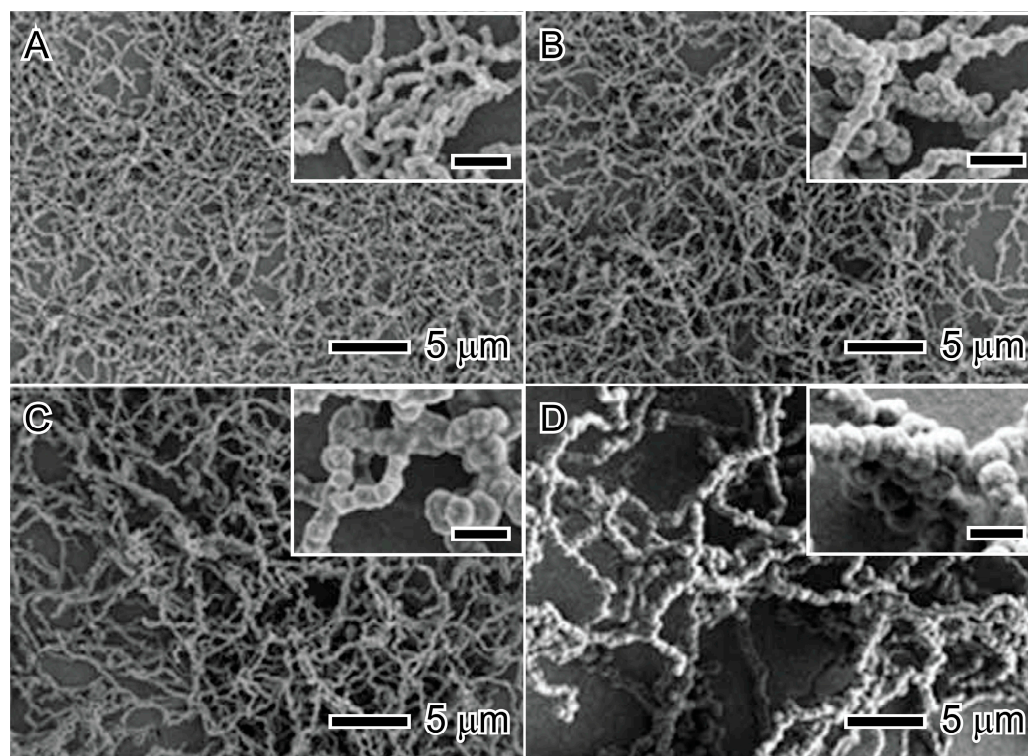
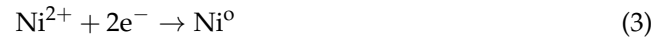


Figure 3. Influence of precursor concentration on the chain-like nanostructured material size: 5 mM (A), 10 mM (B), 20 mM (C), and 50 mM (D). Scale bars in inset images represent 500 nm. Reproduced with permission from [33], Royal Society of Chemistry, 2012.

2.1. Reducing Agent

The reducing agent has the function of reducing the nickel ion (Ni^{2+}) to the nickel atom (Ni^0) by the global redox reaction (Equation (2)), in which the nickel ion is reduced to a nickel atom, receiving two electrons from the reducing agent (R_{red}) (Equation (3)). The reducing agent is converted to oxidized species (R_{oxi}) (Equation (4)). Each reductant molecule exhibits unique behavior to promote different reduction ratios in the number of electrons donated (n) and the reduction potential, influencing the final nanoparticle.

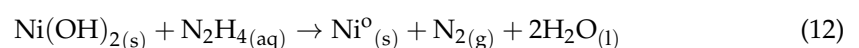
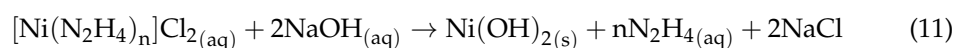
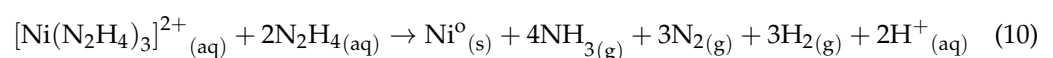
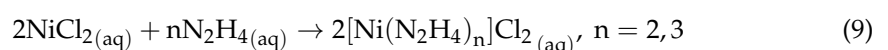
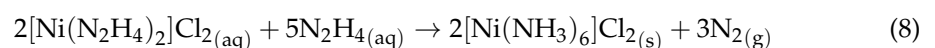
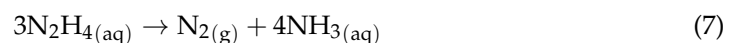
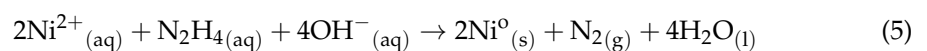
Some examples of reducing agents are hydrazine (N_2H_4), polyalcohols, sodium borohydride (NaBH_4), sodium formaldehyde sulfoxylate, benzyl diethylenetriamine, sodium hypophosphite (NaH_2PO_2), borane tributylamine, and oleylamine [30,32,35–41].

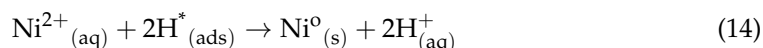


Hydrazine (N_2H_4) is a widely used reducing agent due to its strong reducing potential, which is potentialized in the presence of alkaline medium to synthesis of nickel nanoparticles. However, the mechanism to form nickel nanoparticles can be more complex than the global reaction (Equation (5)) [42]. It occurs through a complexation reaction, where, depending on the ratio of $[\text{N}_2\text{H}_4]/[\text{Ni}^{2+}]$, it can form tris(hydrazine) nickel (II) chloride ($[\text{Ni}(\text{N}_2\text{H}_4)_3]\text{Cl}_2$), bis(hydrazine) nickel(II) chloride ($[\text{Ni}(\text{N}_2\text{H}_4)_2]\text{Cl}_2$), and hexa-ammine nickel (II) chloride ($[\text{Ni}(\text{NH}_3)_6]\text{Cl}_2$), and many pathways.

The ratio of $[\text{N}_2\text{H}_4]/[\text{Ni}^{2+}]$ is determinant to synthesizing well-defined nickel nanoparticles. The ratio $[\text{N}_2\text{H}_4]/[\text{Ni}^{2+}] = 1$ is the minimum ratio to form metallic nickel, exhibiting a wide size distribution and agglomeration due to Van der Waals forces and magnetic attractions [33,43]. When $[\text{N}_2\text{H}_4]/[\text{Ni}^{2+}] \leq 3$, the amount of N_2H_4 is not enough to reduce all the Ni^{2+} to Ni^0 . N_2H_4 is catalytically decomposed on the nickel surface to produce N_2 and H_2 (Equation (6)) and N_2 and NH_3 (Equation (7)) [10,43,44]. Additionally, a light violet complex ($[\text{Ni}(\text{NH}_3)_6]\text{Cl}_2$) is formed (Equation (8)) [10,45]. The reaction between NiCl_2 and N_2H_4 produces $[\text{Ni}(\text{N}_2\text{H}_4)_n]\text{Cl}_2$, $n = 2$ or 3 (Equation (9)). When $[\text{N}_2\text{H}_4]/[\text{Ni}^{2+}] > 4.5$, a sky-blue-colored complex ($[\text{Ni}(\text{N}_2\text{H}_4)_2]\text{Cl}_2$) is formed [46], and when $[\text{N}_2\text{H}_4]/[\text{Ni}^{2+}] < 3$, a pink-colored complex ($[\text{Ni}(\text{N}_2\text{H}_4)_3]\text{Cl}_2$) is formed [10,43,45,47,48]. Until the solution has both complexes, the nanoparticles will be uncontrolled in size and morphology due to the difference between the reaction kinetics of the complexes. The nanoparticles will exhibit controlled size and morphology when $[\text{N}_2\text{H}_4]/[\text{Ni}^{2+}] < 4.5$.

However, the reaction can be based on the absence of OH^- to reduce the nickel complex to metallic nickel by direct hydrazine reduction (Equation (10)) [28], and the presence of OH^- in the reaction medium produces a color change to a gray color, indicating the ligand exchange of Cl^- ion by OH^- to form the nickel hydroxide ($\text{Ni}(\text{OH})_2$) (Equation (11)) [10,43,45,48]. Subsequently, the color changes from gray to black due to the subsequent reduction by hydrazine (Equation (12)) [43]. However, the remaining hydrazine reacts with OH^- in solution to generate electrons (Equation (13)) and water to produce adsorbed hydrogen atoms (H^*). The nuclei formed can act as an active center and site for the adsorption of hydrogen atoms, capturing Ni^{2+} ions from the solution and reacting to form Ni^0 (Equation (14)) [10,49].





Alcohols and polyalcohols (polyols) are attractive compounds in synthesized metal nanoparticles due to their multiple roles in a reaction, acting as a solvent, stabilizer, and/or reducing agent [50,51]. The polyol reduction mechanism strongly depends on the temperature and generates different products that reflect on nickel synthesis with well-defined morphology nanoparticles [51,52]. Alcohols and polyols are generally used to reduce metal ions, and an aldehyde is generated as a by-product of H^+ ions (Equation (15)). When ethylene glycol (EG) is used as a reducing agent, the reaction is conducted at a temperature above 160 °C, and EG is dehydrated to generate acetaldehyde (Equation (16)). In sequence, acetaldehyde is responsible for reducing metal ions, accompanied by its oxidation to diacetyl (Equation (17)) [53]. In the range from 140 °C to 160 °C, the EG heating in air generates glycolaldehyde (Equation (18)) and then serves as a reductant for metal ions while it is oxidized to glyoxal (Equation (19)) [32,50,54]. When the reaction temperature is below 140 °C, EG acts as a reductant by itself, forming glycolaldehyde as the oxidized product (Equation (20)) [50].

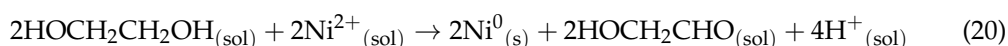
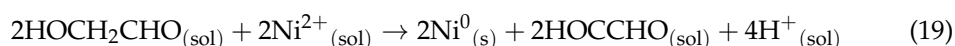
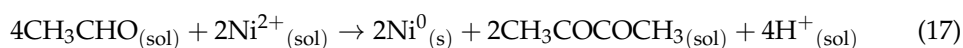
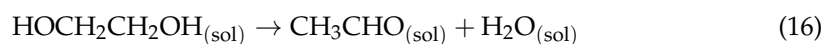
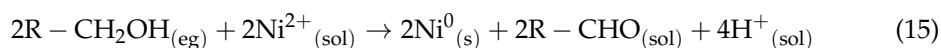


Figure 4 shows the ethylene glycol reduction mechanism of nickel [51]. Kyler et al. propose the reaction mechanism by theoretical modeling, testing different complexes between nickel and EG [51]. In Figure 4A, the graphical representation shows the change in energy ΔE ($\text{kcal}\cdot\text{mol}^{-1}$) during the reduction reaction between EG and NiCl_2 . In this process, the metal center forms an intermediate phase with EG, and the reduction proceeds by forming the C–O–Ni bond. In the mechanism, when nickel dissolves in glycol, EG acts as ligands to form a Ni-glycolate complex. The solution contains OH^- ions that take the H^+ from the carbon center to form water, leaving two electrons to create a double bond with oxygen and two electrons to reduce the metal center. The reaction results in the production of 2-hydroxyacetaldehyde and 2-hydroxyethanolate (Figure 4B) [51]. However, using only polyol is insufficient to completely reduce all nickel ions and achieve a well-defined shape and dispersity [46,51,55]. In an effort to address this, researchers have explored alternative approaches in the literature to achieve the complete reduction of nickel. These approaches involve introducing additional reducing agents or providing more energy, employing methods such as hydrazine and NaBH_4 , and/or utilizing microwave irradiation [10,22,28,29,32,38,52,56–62].

The polyol method employs various alcohols and polyols, including ethanol, benzyl alcohol, 1,2-propanediol, 1,2-butanediol, ethylene glycol, diethylene glycol, triethylene glycol, tetraethylene glycol, and butylene glycol [32,38,51,61,62]. The choice of alcohols and polyols introduces particle size and shape variation attributed to the reduction potentials of these compounds serving as the reductant agent [50,63,64]. As reported by Biacchi and Schaak, the applied potential required for the initiation of the polyol, and thus the oxidation potential of the polyols at room temperature and 60 °C, decreases in the order of ethylene glycol > diethylene glycol > triethylene glycol > tetraethylene glycol. This trend is likely due to the enhanced electronic stability of alcohols provided by the higher intermolecular bonding facilitated by the ether functionalities [63].

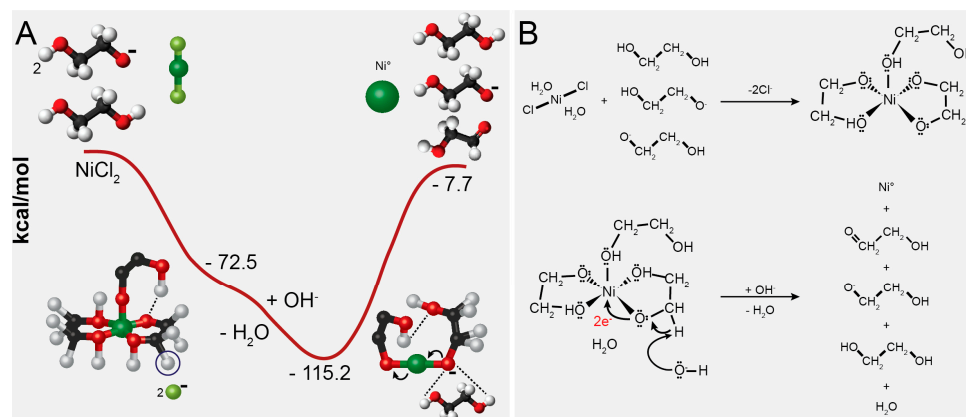


Figure 4. The plot of the calculated change in energy (A) and reaction mechanism of Ni^{2+} reduction by the ethylene glycol (B). Reproduced with permission from [51], American Chemical Society Publications, 2011.

Figure 5 presents examples of nickel nanoparticles synthesized using the polyol method with different polyols. The upper images were produced with the same quantity of NiCl_2 as the precursor, trioctylphosphine oxide (TOPO), as the capping agent, hydrazine as the reducing agent, and microwave irradiation at $160\text{ }^\circ\text{C}$ (left and middle) and $200\text{ }^\circ\text{C}$ (right), utilizing either ethylene glycol (Figure 5C) or diethylene glycol (Figure 5D,E) as the solvent. When ethylene glycol is present, nanowires are formed with a length of several micrometers and a width of 120 nm. The rough surface is a result of small nanoparticle agglomeration through the oriented attachment mechanism associated with Ostwald ripening in an anisotropic growth [64]. On the other hand, in the presence of diethylene glycol, agglomerated spherical nanoparticles are observed. This suggests that the glycol structure influences the synthesis, a correlation that becomes evident when analyzing the molecular structures of both ethylene glycol and diethylene glycol (Figure 5A,B).

Figure 4 demonstrates that the hydroxyl group connects ethylene glycol to nickel, creating a cyclic molecule with the metal. In diethylene glycol, these connections are formed by the terminal hydroxyl groups due to stress in the structure of the molecule, leading to the detachment of the ether group in the middle of the molecule. This ether group interacts with other nickel complexes, inducing agglomeration. In the experiments conducted at $200\text{ }^\circ\text{C}$, the nanoparticles still agglomerate, but with less intensity and a noticeable chain morphology (Figure 5E). The interpretation of this phenomenon is that the higher temperature weakens the interaction of the ether group with the nickel complex, allowing for greater freedom and, consequently, less agglomeration of the nanoparticles [22].

The flower-like (Figure 5F) and urchin-like (Figure 5G) nanostructured materials were synthesized using a surfactant-free solvothermal polyol method. The process involved NiCl_2 as the precursor, NaOH as the precipitant agent, a small amount of water (or none), and 1,2-propanediol as the reducing agent and solvent [32]. The nanostructures are formed by reducing Ni^{2+} by 1,2-propanediol according to Equations (18) and (19), resulting in the generation of nuclei and random agglomeration, as illustrated in Figure 2. This process produces nanospheres with a rough surface. The concentration of water in the reaction alters the growth kinetics, shifting Equation (18) to the left and reducing $\text{CH}_3\text{CH}_2\text{CHO}$. Propanal serves as the actual reducing agent for nickel, and an increase in water content effectively slows down the reduction kinetics. Once the nanosphere is formed, the reaction becomes thermodynamically dominated rather than kinetic. This leads to an anisotropic growth direction of a magnetic crystalline, minimizing anisotropic magnetic energy and forming urchin-like nanopagodas with a diameter of $1\text{ }\mu\text{m}$ [32,65–67]. In contrast, during quasi-equilibrium growth, the nanoplates grow on high-energy facets {111} to minimize total surface free energy according to Ostwald ripening and the Gibbs–Thomson law. This results in the formation of flower-like nanostructured material with a diameter of $1.5\text{ }\mu\text{m}$ and a thickness of 10 nm [32,68].

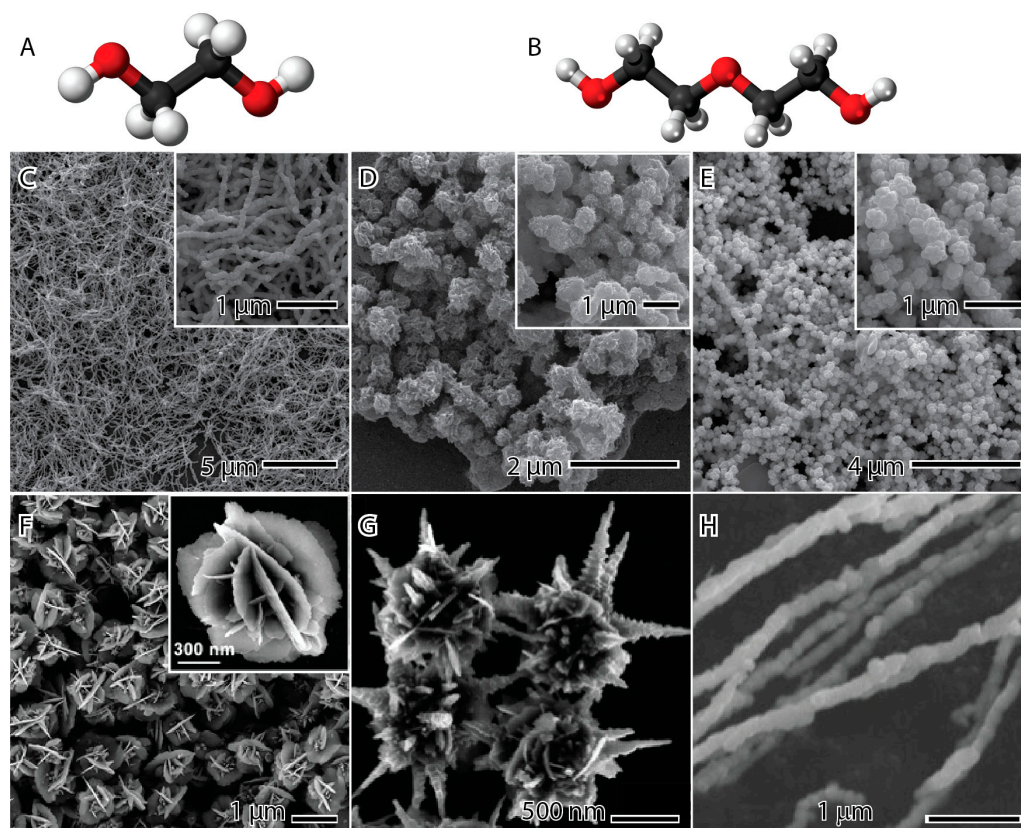


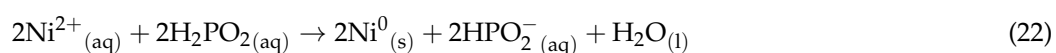
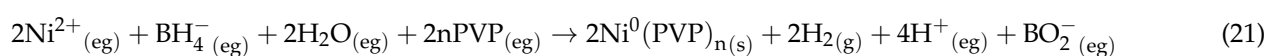
Figure 5. Ethylene glycol (A) and diethylene glycol (B) molecules, where white, red, and black balls represent the hydrogen, oxygen, and carbon atoms. Nickel nanoparticles synthesized by the polyol method in the presence of ethylene glycol (C), diethylene glycol (D,E), 1,2-propanediol (F), 1,2-propanediol and water (G), and ethylene glycol (H). The images (C–E) are reproduced with permission from [62], American Chemical Society Publications, 2008. The images (F–G) are reproduced with permission from [32], Royal Society of Chemistry, 2011. The image (H) is reproduced with permission from [69], Elsevier, 2009.

Figure 5H displays nickel nanowires synthesized using a magnetic field-assisted polyol method. The process involves NiSO_4 as the precursor, NaOH as the pH modifier agent, hydrazine as the reducing agent, and ethylene glycol as the solvent [69]. The magnetic field-assisted synthesis method is known for synthesizing magnetic materials with ferromagnetic or paramagnetic properties, such as iron, nickel, cobalt, copper, and manganese. When magnetic nanoparticles are exposed to a magnetic field, they behave as permanent magnets due to magnetic interaction [70]. This method typically produces one-dimensional (1D) particles like wires and rods due to the magnetic particles aligning along the magnetic line force [67]. In the synthesis process, the precursor is first added to the solution, applied to the magnetic field, and then reduced. This leads to the formation of spiky nanowires, with the nucleus dispersed in the solution and fixed in the wire, resulting in spiky protuberances on the surface. The magnetic field is applied to the solution in the second synthesis, and the precursor is dropped into it. This slight difference in the synthesis process results in a smoother surface on the nanowire. This is due to the droplet-induced process bringing the nickel nuclei closer to each other, promoting a more even distribution [69,71,72].

Other reducing agents have been employed more discreetly than those discussed above, indicating a significant potential to expand the knowledge frontier of synthesizing nickel nanoparticles. Sodium borohydride (NaBH_4) stands out as a more potent reducing agent compared to hydrazine (N_2H_4), with reduction potentials of 1.24 V and 1.16 V, respectively, and the capability to donate double the number of electrons (8 electrons). As demonstrated in Figure 2, when the nucleation and growth processes are well separated,

particle size can be controlled. Fast nucleation produces small particles and a high concentration of particles by consuming all ion precursors simultaneously, while slow nucleation results in large particles and a low concentration of particles due to gradual reduction over time [73].

Supporting this argument, Figure 6A illustrates using NaBH_4 as a potent reducing agent in a polyol method with PVP as a capping agent. In this case, a significant number of nickel ion precursors are simultaneously converted into nuclei (Equation (21)), promoting a narrow size distribution and small particles with a diameter ranging from 3.4 to 3.8 nm, along with a high concentration of nanoparticles. Additionally, the presence of PVP and ethylene glycol stabilizes the nucleus, preventing agglomeration [56]. Similarly, nickel nanoparticles were synthesized with a narrow size distribution in an aqueous solution with oleic acid and sodium dodecyl sulfate (SDS) as surfactants (Figure 6B). This outcome is attributed to the well-controlled nucleation and growth processes facilitated by NaBH_4 and the protective agents that prevent agglomeration [25].



On the contrary, sodium hypophosphite (NaH_2PO_2) acts as a weaker reducing agent compared to hydrazine. This results in a slower nucleation process, leading to larger particle size and lower particle concentration. Being a soft reductant, it facilitates an extended nucleation process, as depicted in Figure 6C. A considerable number of nuclei are formed during the initial stages of nucleation, resulting in the creation of smaller particles. As the reaction continues, more nickel atoms are reduced and adsorbed onto the primary nuclei. These nuclei act as seeds in the Ostwald repeating process, ultimately producing larger and hierarchical particles [74].

Another approach utilizing NaH_2PO_4 has been employed to synthesize hollow nanoparticles (Figure 6D). Typically, the soft template for micellar formation can be generated through an emulsion system with water-in-oil (W/O) [75], polymers [30], or counterions, such as dodecyl sulfate in $\text{Ni}(\text{DS})_2$ [76]. Nickel ions are located around the micelle due to electrostatic forces at the micelle interface. The reduction of nickel occurs upon adding the reductant to the solution (Equation (22)) [37], leading to the formation of the shell [30,75,76]. Notably, the reducing agent must be soft and reduce the metal at a lower ratio than nickel adsorbed on the micelle surface. Otherwise, it may result in bulk nanoparticles, such as flower- or wire-like nanoparticles [76]. Hollow nickel nanoparticles were synthesized using citric acid in an alternative method. The use of bis(N- α -amido-glycylglycine)-1,7-heptane dicarboxylate (HG12) led to the formation of a peptide nanotube. Citric acid, acting as an intermediate reductant weaker than hydrazine but stronger than NaH_2PO_4 , resulted in nanoparticles with a size of 30 nm on the nanotube surface instead of covering the tube with a single shell [77].

In nanoparticle synthesis, the choice of reducing agent plays a crucial role in determining the size, morphology, and properties of the resulting nanoparticles. Reductant agents can be categorized into three groups based on their reduction potential strength: strong, medium, and weak. Strong reductants, such as hydrazine and NaBH_4 , are known for inducing burst nucleation, where numerous growth species form simultaneously, leading to the rapid generation of small and uniform nuclei, smaller than 10 nm. Adjusting the pH level can enhance the reduction potential of these reductant agents.

Medium-strength reductants, including polyols and citric acid, offer a moderate reduction potential and reaction rate, resulting in nanoparticles with tailored sizes (approximately 70 nm) and morphologies. Polyols serve multiple roles as reducing agents, solvents, and stabilizing agents, striking a balance between reduction capability and reaction control. The polyol reduction mechanism, influenced by factors like temperature and precursor concentration, yields nanoparticles with diverse morphologies. Additionally, variations in

the reduction potentials of different alcohols and polyols impact their suitability as reducing agents, thereby influencing the nanoparticle synthesis process. Weak reductant agents, such as ascorbic acid and sodium hypophosphite (NaH_2PO_2), possess lower reduction potentials and slower reaction rates. These agents are often utilized for the gradual reduction of metal ions, leading to slower nucleation and growth processes. Consequently, weak reductants require longer reaction times to convert all precursors, potentially resulting in the formation of larger nanoparticles.

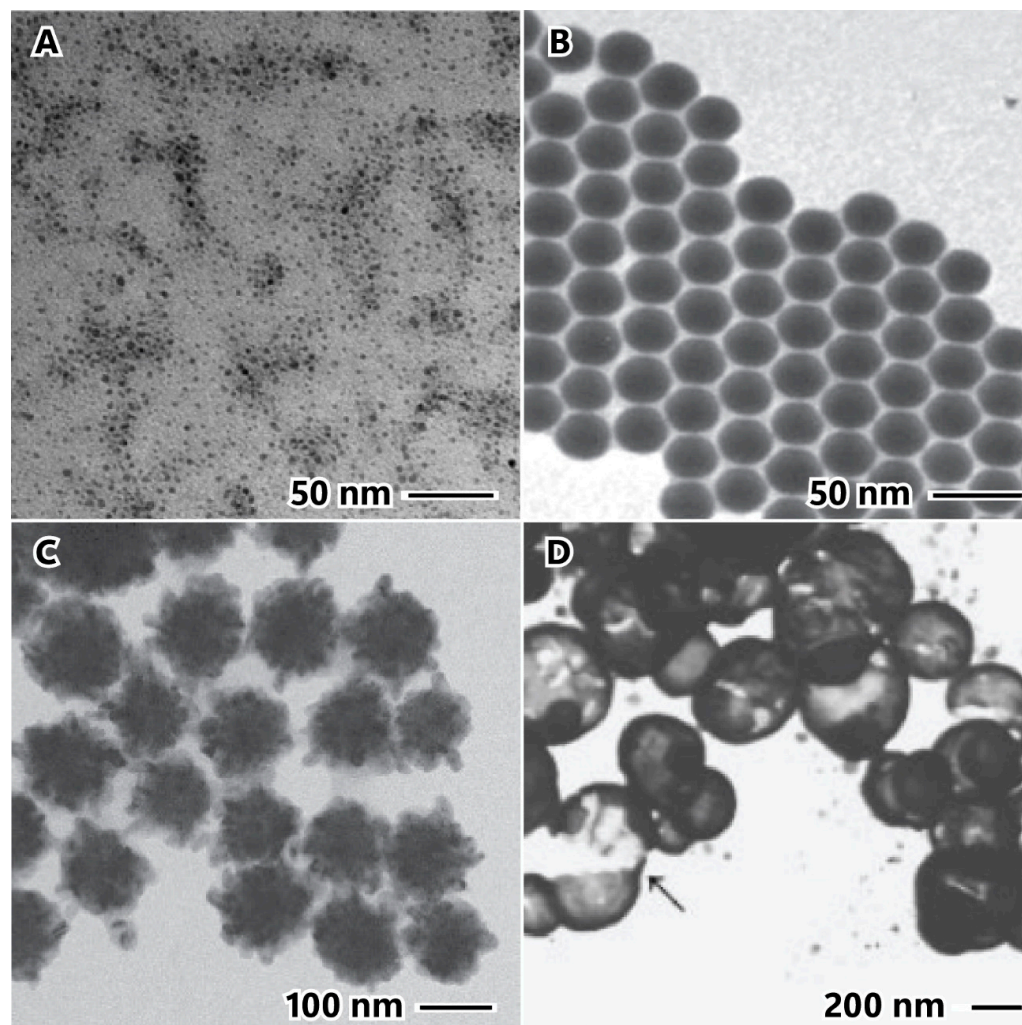


Figure 6. Reducing agents: sodium borohydride in polyol method (A), aqueous solution (B), sodium hypophosphite produced in bulk nanoparticles (C), and hollow nanoparticles (D), where arrow points to a broken hollow nanoparticle. The image (A) is reproduced with permission from [56], Elsevier, 2007. The image (B) is reproduced with permission from [25], American Chemical Society Publications, 2009. The image (C) is reproduced with permission from [74], Elsevier, 2010. The image (D) is reproduced with permission from [30], John Wiley and Sons, 2003.

2.2. Stabilizing Agent

Stabilizing agents can take the form of additives, including organic molecules, polymers, or surfactants, as well as ions, such as counterions of precursors that bind to specific crystalline surfaces. These agents play a crucial role in steric stabilization, protecting against uncontrolled growth. However, it is important to note that the exposed plane tends to grow when the surface is stabilized, as illustrated in Figure 7 [48,49]. This phenomenon is rooted in nucleation and growth theory, as depicted by the LaMer curve [50]. In this theory, a crystal is an ion that undergoes reduction to produce metallic atoms, promoting their

aggregation to form small nuclei through self-nucleation [51]. As a result, the concentration of atoms decreases while the cluster concentration increases, leading to an increase in nuclei size, ultimately forming tiny crystals. The role of the stabilizing agent is crucial for controlling the shape and/or size because the crystalline surface is well defined, and the stabilizing agent can perform more efficiently. In Figure 7a, crystal growth without a stabilizing agent is shown, where the nuclei are incorporated onto all crystal surfaces, resulting in uniform growth. In Figure 7b, a moderate amount of stabilizing agent is used to control the synthesis to form a cube. In this example, the exposed planes are (111) and (100), and the stabilizing agent preferentially interacts with the (100) plane, inhibiting its growth. As a result, the exposed (111) plane grows easily until the desired surface is achieved. In Figure 7c, an excessive amount of stabilizing agent is employed, fixing, and protecting all exposed surfaces. This inhibits crystal growth, leading to the formation of smaller particles.

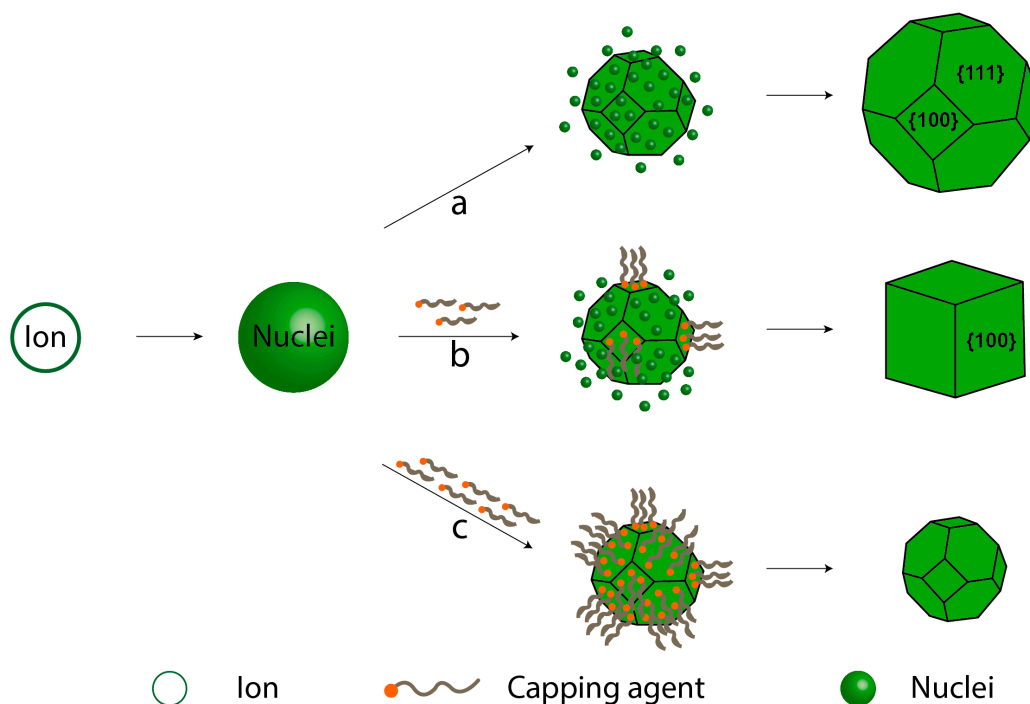


Figure 7. Control over nanocrystal shape using capping agents: (a) no capping agent, (b) a moderate amount of capping agent, and (c) a large amount of capping agent.

As indicated earlier, nanoparticles exhibit high surface energy, resulting in thermodynamic instability at the surface and a propensity to minimize surface energy through aggregation, driven by the reduction of surface area. Self-aggregation can be enhanced by van der Waals forces and magnetic dipole–dipole interactions, particularly in magnetic materials [78–80]. However, stabilizing agents can counteract this tendency by utilizing π – π interactions, electrostatic forces, and hydrogen bonding to prevent agglomeration. They play a crucial role in organizing the building blocks into a controlled morphology and size [72]. Numerous stabilizing agents, including surfactants and other compounds, can be employed in nickel synthesis, for example, cetyltrimethylammonium bromide (CTAB), tetraethylammonium bromide (TBAB), tetrabutylammonium bromide (TEAB), tetra dodecyl ammonium bromide (TC₁₂AB), citric acid, sodium dodecyl sulfonate (SDS), Tween 40, Tween 80, D-sorbitol, PEG 6000, sodium carboxyl methylcellulose (Na-CMC), hydroxyethyl carboxymethyl cellulose (HECMC), trioctylphosphine oxide (TOPO), trioctylphosphine (TOP), and poly(vinylpyrrolidone) (PVP) [21,26,34,42,62,73,76,81–88].

The main function of the stabilizing agent is to prevent particle agglomeration and stabilize the surface charge of the nanoparticles. A critical consideration in selecting the stabilizing agent is its polarity and electrical charge characteristics, which can be categorized

as cationic, anionic, and nonionic. These characteristics can be expressed by the Critical Packing Parameter (CPP), representing the minimum interfacial area occupied by the stabilizer molecule. The CPP equation is defined as depicted in Equation (23), where v is the volume of the hydrophobic chain, l_c is the length of the hydrophobic chain, and a_0 is the interfacial area occupied by the hydrophilic head group [29,81]. Estimating this parameter can provide insights into molecular packing and the preferred stabilizer structure, whether spherical or cylindrical. This phenomenon is exemplified using cetyltrimethylammonium bromide (CTAB) in a polyol method [29]. CTAB exhibits two Critical Micelle Concentrations (CMC) at 2 mM and 20 mM. At concentrations below 2 mM, nanoparticles form with a spherical-like shape, while concentrations above 20 mM result in nanoparticles with a wire-like shape. This behavior can be explained by the tendency of the hydrophobic group (tail) to minimize contact with polar molecules like water, while the hydrophilic group (head) maximizes contact [81].

$$\text{CPP} = \frac{v}{a_0 l_c} \quad (23)$$

As previously mentioned, the head group in the surfactant plays a crucial role in nanoparticle synthesis, influencing the morphology of micelles and the interaction of the surfactant with ions, intermediates, and particle surfaces. The charge in the head group in the surfactant can be cationic (X^+), anionic (X^-), nonionic (X°), and zwitterionic (X^+Y^-), and different choices during nickel synthesis can impact the result. Notable examples include cationic surfactants like CTAB, TBAB, TEAB, and TC_{12}AB , anionic surfactants like SDS, and nonionic surfactants such as TOP, Tween, and D-sorbitol. Given that the charge of nickel ions (Ni^{2+}) is positive and that $\text{Ni}(\text{OH})_2$ is an intermediate with a neutral charge in the reaction solution, the interaction between surfactants and these entities can influence the synthesis process. For instance, CTAB, a cationic surfactant, is known to reduce mass transfer and the reduction process [24,82,83]. In the reaction system, CTAB forms CTA^+ and faces challenges in effectively coating Ni^{2+} due to electrostatic repulsion [83]. Under alkaline conditions, CTAB may interact to cover $\text{Ni}(\text{OH})_2$ or form $\text{CTA}^- \text{Ni}(\text{OH})_4$, where the latter is composed of $\text{Ni}(\text{OH})_4^{2-}$. This interaction with CTAB can pack the $\text{Ni}(\text{OH})_2$, preventing its reduction to Ni° [24,71,82,83]. In general, stabilizing agents interact with nickel ions, $\text{Ni}(\text{OH})_2$, and nickel particles through the more energetic groups on molecules, such as C–O, –OH, N^+ , S–O, P=O [24,25,34,80,84–87].

The stabilizing agent plays a crucial role in the synthesis of nanoparticles. Figure 8 illustrates examples of stabilizing agents utilized in the synthesis of nickel nanostructured materials. The impact of stabilizing agents in hydrothermal syntheses is demonstrated without cetyltrimethylammonium bromide (CTAB) (Figure 8A) and with CTAB (Figure 8B). In the absence of CTAB, crystals can grow in all directions, forming a rod (secondary particle) within the primary particle. However, when CTAB is present, the surfactant forms a layer on the initial growth surface, preventing growth around the thorn side faces and promoting growth on top where there is no surfactant. This results in the formation of urchin-like nanobelts due to steric hindrance [24]. Certain organic modifiers can serve a dual function. For instance, ethylene glycol can act as both a solvent and a stabilizing agent, while citric acid, as shown earlier, serves as a reducing agent and a stabilizing agent in this example. In this case, hierarchical nanostructured materials were synthesized using an ultrasonic alcohol method with hydrazine and citric acid. The combination of these reductant molecules initially formed small particles measuring 9 nm. With citric acid preventing agglomeration, the nanoparticles aggregated due to magnetic dipole interaction, reducing the anisotropic magnetic energy, and forming secondary spherical particles with a diameter of 254 nm [84].

The number and type of anchors on the polymer stabilizing agent can indicate the strength of the interaction between the stabilizing agent and the particle surface, while the size of the polymer can reflect the degree of coverage and protection. In Figure 8, two PVP chain lengths are depicted, with molecular weights of 10,000 (Figure 8D) [55] and 30,000 (Figure 8E) [62]. PVP has one anchor point (C=O) in each monomer of the molecule

chain. In PVP-10,000, the particle surface appears rough with protrusions, indicating a less protective layer that allows nuclei diffusion and surface particle growth. Conversely, PVP-30,000 exhibits a smooth particle surface, suggesting that a longer polymer chain better prevents nucleus diffusion to the surface and promotes growth. Hydroxyethyl cellulose (HEC) (Figure 8F) [85] and Tween 80 (Figure 8G) [21] possess multiple anchors (C–O–C) or/and (C=O), enabling these polymers to be anchored at multiple points. This allows the polymers to interconnect on various faces in each HEC molecule, forming a sponge nanoflower.

Certain stabilizing agents exhibit a preference for binding to the {111} crystallographic plane due to the lower activation energy associated with this plane. By passivating the {111} plane, growth occurs anisotropically in the <110> plane, which has higher energy [72,89–91]. Figure 8H illustrates triangular nanoplates synthesized through a thermal decomposition method utilizing oleic acid, oleylamine, and octadecene. Initially, small triangular nanoplates nucleate within the {111} plane and then grow along the <110> direction, resulting in the formation of larger triangular nanoplates. These small particles align along the <110> lateral planes, connecting and growing into large triangular and/or hexagonal nanoplates [90].

Another example is Figure 8I, which shows the flower-like nanostructured materials with hexagonal columnar petals synthesized by the alcohol method using NaOH, hydrazine, and dimethylglyoxime (DMG) as the stabilizing agent. This hierarchical structure is formed by a spherical particle as the primary structure, followed by the confinement of DMG in hexagonal protrusions on the surface of the sphere to form the initial hexagonal nanoplates. The DMG is absorbed on the (111) planes and passivates to form the tops and bottoms of the hexagonal nanoplates, unaffected on the six side (110) planes. The columns are formed by well-aligning the tops and bottoms of the hexagonal plates (inset Figure 8I) due to magnetic interactions, resulting in a (111) column growth [72].

In summary, the stabilizing agent is a relevant variable in the synthesis of nickel nanoparticles by preventing agglomeration and controlling surface charge, size, and morphology. These agents, ranging from organic molecules to polymers and ions, employ various mechanisms such as steric hindrance and electrostatic forces to maintain particle dispersion and stability. The choice of stabilizing agent is crucial, considering factors like polarity and charge characteristics, which influence their interaction with particle surfaces and intermediates during synthesis. For instance, cationic surfactants like CTAB can hinder mass transfer and the reduction process, impacting the morphology and size of nanoparticles. Additionally, the number and type of anchors on polymer stabilizing agents dictate the strength of interaction and degree of surface coverage, thus influencing particle growth and morphology. Certain stabilizing agents exhibit a preference for binding to specific crystallographic planes, directing anisotropic growth and resulting in unique nanostructures. Overall, understanding the interplay between stabilizing agents and nanoparticles is essential for tailoring synthesis processes and achieving desired material properties and structures.

2.3. Reaction Temperature

The temperature represents a significant influence on the size, morphology, and properties of the synthesis of nickel nanoparticles. Temperature impacts reaction kinetics, nucleation, and growth rates, thereby influencing the particle size distribution, morphology, and properties of the nickel nanoparticles [92–95]. Elevated temperatures often accelerate reaction rates, leading to faster nucleation and subsequent particle growth, which can result in larger nanoparticles with distinct morphologies [94]. Conversely, lower temperatures tend to impede reaction kinetics, promoting controlled nucleation and growth, ultimately yielding smaller and more uniform nanoparticles [94].

Additionally, temperature exerts a profound influence on the thermodynamics of nanoparticle formation. The energy landscape of the synthesis process is intricately linked to temperature, affecting the stability and crystallinity of the resulting nanoparticles [93].

Higher temperatures may facilitate the overcoming of energy barriers, leading to the formation of more thermodynamically stable structures. On the other hand, lower temperatures can promote the retention of metastable phases. This thermodynamic interplay not only governs the structural properties of the nanoparticles but also plays a crucial role in determining their long-term stability and performance in various applications [96].

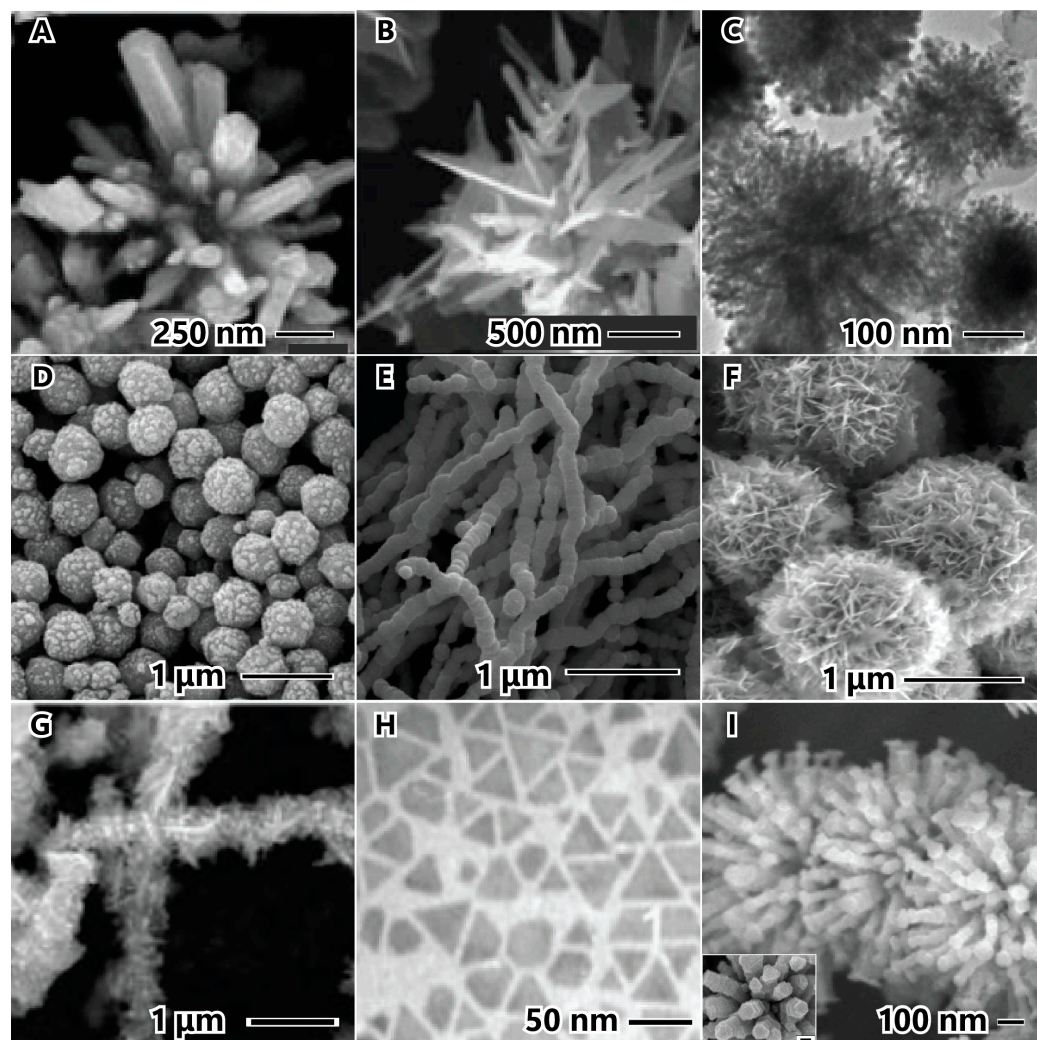


Figure 8. Stabilizing agent employed in synthesis of nickel nanoparticles. Nickel nanoparticles without (A) CTBA, and with CTAB (B), hydroxyethyl cellulose (C), PVP (MW 10,000) (D), PVP (MW 30,000) (E), citric acid (F), Tween 80 (G), octadecene (H), and dimethylglyoxime (I). The images (A) and (B) are reproduced with permission from [24], Elsevier, 2006. The image (C) is reproduced with permission from [84], American Chemical Society, 2009. The image (D) is reproduced with permission from [55], Elsevier, 2005. The image (E) is reproduced with permission from [62], American Chemical Society, 2008. The image (F) is reproduced with permission from [85], Elsevier, 2014. The image (G) is reproduced with permission from [21], Elsevier, 2018. The image (H) is reproduced with permission from [90], American Chemical Society, 2007. The image (I) is reproduced with permission from [72], American Chemical Society, 2007.

The temperature also influences the degree of freedom in atom mobility within nanoparticles, playing a decisive role in shaping their properties [97]. At elevated temperatures, the increased kinetic energy of atoms promotes greater mobility, facilitating dynamic processes such as nucleation, growth, and rearrangement. This heightened degree of freedom allows atoms the exploration of a broader range of positions and orientations, influencing the size, morphology, and crystal structure of nanoparticles [98].

As an example of the influence of temperature on the synthesis of nickel nanoparticles, Bai et al. reported the synthesis of nickel nanoparticles at different temperatures to produce nanostars and nanospheres, as depicted in Figure 9 [98]. The nickel nanoparticles were synthesized using a solvothermal method with ethanol as a solvent, hydrazine as a reducing agent, and NaOH to increase the reduction potential of the reducing agent. The synthetic methodology naturally presents high kinetic conditions. At lower temperatures (60 °C), nanostars with well-defined pronounced arms were produced. At 60 °C (Figure 9A), the reaction medium exhibits a lower degree of freedom of mobility of growth species, which are anchored in the first site with higher energy to grow the arms. However, after increasing the temperature to elevated values, such as 100 °C (Figure 9B) and 140 °C (Figure 9C), the spikes become smaller and with lower definition, forming a spherical morphology at 180 °C (Figure 9D). This indicates that the degree of freedom of the reaction is increasing, and the growth species can have greater mobility on the nanostructured material surface to minimize the free energy of the system [62,98].

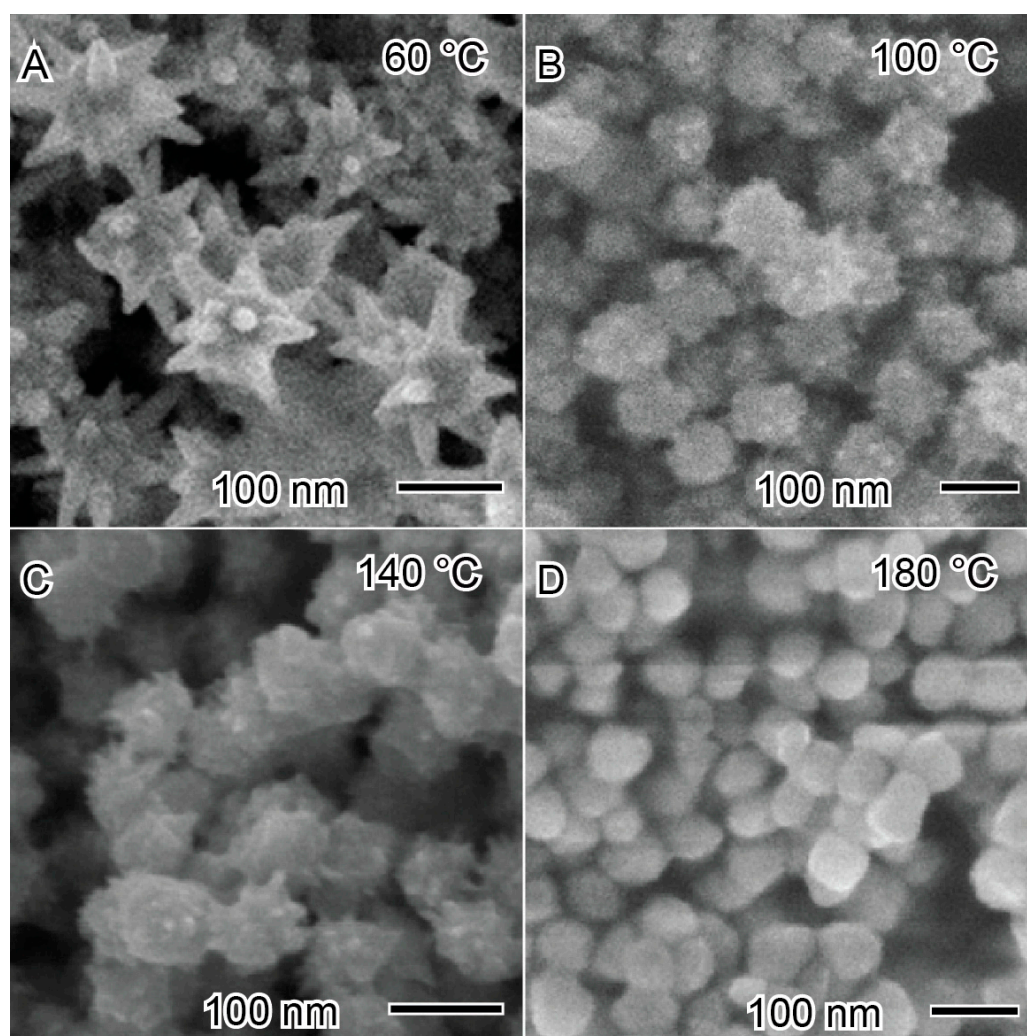


Figure 9. Influence of temperature in the synthesis of nickel nanoparticles at (A) 60 °C, (B) 100 °C, (C) 140 °C, and (D) 180 °C. Reproduced with permission from [98], Elsevier, 2008.

In summary, the reaction temperature is a crucial factor in the synthesis of nickel nanoparticles by controlling the size, morphology, and properties. Elevated temperatures typically accelerate reaction rates, resulting in faster nucleation and particle growth, ultimately yielding larger nanoparticles with distinctive morphologies. Conversely, lower

temperatures hinder reaction kinetics, promoting controlled nucleation and growth, leading to the formation of smaller and more uniform nanoparticles.

3. Purification

The purification process in the synthesis of nanoparticles is a crucial step to ensure the quality, uniformity, and functionality of the resulting nanoparticles and should not be neglected, and should be performed with careful consideration. As discussed above, the nickel nanoparticles are synthesized through different synthesis methods that carry by-products and unreacted components at the end of the synthesis, which are impurities in the purification step. The presence of these contaminants can significantly impact the stability, physicochemical properties, and applicability of the nanoparticles. Storing nanoparticles in the reactional medium can ensure that the nanoparticles continue reacting with the components of the synthesis and growth mechanism, such as Ostwald ripening and intraparticle ripening, which can work to minimize the surface energy of the nanoparticle, potentially changing the size, morphology, and properties. Moreover, the physicochemical properties of the nanoparticles are strongly dependent on a clear surface to exhibit their full potential [99].

In general, nanoparticles can be purified using various methodologies, including centrifugation, magnetic separation, membrane separation (filtration, ultrafiltration, and dialysis), chromatography methods, and thermal treatment purification [96,99–102]. However, the specific purification method for each class of nanoparticles may vary. The most common method for purifying nanoparticles is centrifugation, wherein the nanoparticle suspension undergoes high-speed rotation to separate the nanoparticles by sedimentation, based on differences in size, density, and shape, from surrounding unwanted impurities in the supernatant. Centrifugation can isolate nanoparticles with a specific size distribution, contributing to the homogeneity of the nanoparticles through parameters such as rotational speed, centrifugation time, temperature, solvent, viscosity of the medium, and the number of centrifugation cycles [99,102].

Magnetic separation is a valuable methodology that strategically exploits the magnetic properties to purify magnetic nanoparticles, such as nickel nanoparticles [102–104]. The nanoparticle suspension is exposed to an external magnetic field, causing the magnetic nanoparticles to be selectively separated from the solution while non-magnetic impurities remain dispersed in the supernatant [92]. Magnetic separation can be controlled through factors like magnetic field strength, distance from the magnetic source, duration of magnetic exposure, viscosity of the medium, and temperature [99,102,104].

Another relevant aspect of purification is the affinity and chemical nature of the impurities and solvents used in the separation process. Unwanted components can be classified into ionic and molecular components, and the separation of molecular components can be based on solubility, polarity, or dielectric constant [92,105]. Ionic components, which are soluble in water, can be completely removed using water as a solvent with successive separation cycles [103,106]. Molecular compounds can be eliminated using molecular solvents such as ethanol, isopropyl alcohol, and acetone, depending on the solubility, polarity, and dielectric constant of the impurity. In a hypothetical synthesis involving different components with distinct solubility, polarity, and dielectric constant, it is necessary to use solvents with ascending or descending dielectric constants in sequence to enable miscibility between the anterior and posterior solvents [105,106].

4. Conclusions

Significant advances have been made in the synthesis of nickel nanoparticles, with a focus on understanding and manipulating various variables and parameters. This review emphasizes the exploration of physical and chemical factors, including the precursor concentration, characteristics of the reducing agent, reaction temperature, and stabilizing agents, to achieve well-controlled particle size and morphological distribution. The discussion begins with an examination of the nickel salt precursor and its concentration, which

crucially determine the size and morphology of the resulting nanoparticles. Subsequently, the role of the reducing agent, such as hydrazine, polyalcohols, and sodium borohydride, is discussed, highlighting its dual function in reducing nickel ions and stabilizing the reaction. The concentration and nature of the reducing agent play a significant role in shaping the final characteristics of the nanoparticles, necessitating careful selection and optimization for desired structures. The reductant agents can be categorized into three groups based on their reduction potential strength: strong, medium, and weak. Strong reductants, such as hydrazine and NaBH_4 , induce burst nucleation leading to the rapid generation of small (<10 nm) and uniform nuclei. Medium-strength reductants, including polyols and citric acid, offer a moderate reduction potential and reaction rate, resulting in nanoparticles with tailored sizes and morphology. Weak reductant agents, such as ascorbic acid and NaH_2PO_2 , possess lower reduction potentials, resulting in the formation of larger nanoparticles. Stabilizing agents are fundamental in preventing uncontrolled growth and agglomeration through steric or electrostatic stabilization. The choice of stabilizing agents, such as organic molecules, polymers, surfactants, and ions, is influenced by their ability to interact with specific crystalline surfaces, ultimately controlling the synthesis process and resulting in well-defined structures. The impact of reaction temperature on kinetics, nucleation, and growth rates is discussed, providing insights into its influence on the size and morphology of nanoparticles. The thermodynamics of nanoparticle formation is elucidated, demonstrating how temperature affects stability, crystallinity, and long-term performance. Following the synthesis process, the purification step is examined, emphasizing the importance of removing impurities to ensure the quality and uniformity of nickel nanoparticles. Considering factors like rotational speed, magnetic field strength, and solvent characteristics underscores the importance of the purification process. In this context, this review posits that advancements in nickel nanoparticle synthesis, enabling precise tuning of multiple physical and chemical parameters, are pivotal for enhancing our comprehension of, and driving progress in, the fields of chemistry and nanoscience.

Author Contributions: Writing—original draft preparation, F.A.e.S.; writing—review, V.M.M.S.; writing—review and editing, T.S.R. All authors have read and agreed to the published version of the manuscript.

Funding: We are grateful to the Fundação de Amparo à Pesquisa do Estado do Rio de Janeiro (FAPERJ), grant numbers E-26/201.431/2021 and E-26/211.612/2019; to the Conselho Nacional de Desenvolvimento Científico e Tecnológico—CNPq, grant number 317288/2021-0; and to the Coordenação de Aperfeiçoamento de Pessoal de Nível Superior—Brasil (CAPES)—Finance Code 001, grant number 88887.645934/2021-00.

Conflicts of Interest: The authors declare no conflicts of interest.

References

1. Kazuhi, Q.Z.Y.K. Differences in the Extent of Inflammation caused by Intratracheal Exposure to Three Ultrafine Metals: Role of Free Radicals. *J. Toxicol. Environ. Health A* **1998**, *53*, 423–438. [[CrossRef](#)]
2. Zhang, Q.; Kusaka, Y.; Zhu, X.; Sato, K.; Mo, Y.; Kluz, T.; Donaldson, K. Comparative Toxicity of Standard Nickel and Ultrafine Nickel in Lung after Intratracheal Instillation. *J. Occup. Health* **2003**, *45*, 23–30. [[CrossRef](#)]
3. Zhu, F.Q.; Chern, G.W.; Tchernyshyov, O.; Zhu, X.C.; Zhu, J.G.; Chien, C.L. Magnetic Bistability and Controllable Reversal of Asymmetric Ferromagnetic Nanorings. *Phys. Rev. Lett.* **2006**, *96*, 27205. [[CrossRef](#)]
4. Ban, I.; Stergar, J.; Drogenik, M.; Ferk, G.; Makovec, D. Synthesis of Copper–Nickel Nanoparticles Prepared by Mechanical Milling for Use in Magnetic Hyperthermia. *J. Magn. Magn. Mater.* **2011**, *323*, 2254–2258. [[CrossRef](#)]
5. Maynard, A.D.; Kuempel, E.D. Airborne Nanostructured Particles and Occupational Health. *J. Nanopart. Res.* **2005**, *7*, 587–614. [[CrossRef](#)]
6. Wang, S.-F.; Xie, F.; Hu, R.-F. Carbon-Coated Nickel Magnetic Nanoparticles Modified Electrodes as a Sensor for Determination of Acetaminophen. *Sens. Actuators B Chem.* **2007**, *123*, 495–500. [[CrossRef](#)]
7. Lei, D.; Lee, D.-C.; Magasinski, A.; Zhao, E.; Steingart, D.; Yushin, G. Performance Enhancement and Side Reactions in Rechargeable Nickel–Iron Batteries with Nanostructured Electrodes. *ACS Appl. Mater. Interfaces* **2016**, *8*, 2088–2096. [[CrossRef](#)]
8. Bajpai, R.; Roy, S.; Kulshrestha, N.; Rafiee, J.; Koratkar, N.; Misra, D.S. Graphene Supported Nickel Nanoparticle as a Viable Replacement for Platinum in Dye Sensitized Solar Cells. *Nanoscale* **2012**, *4*, 926–930. [[CrossRef](#)] [[PubMed](#)]

9. Ashar, A.; Iqbal, M.; Bhatti, I.A.; Ahmad, M.Z.; Qureshi, K.; Nisar, J.; Bukhari, I.H. Synthesis, Characterization and Photocatalytic Activity of ZnO Flower and Pseudo-Sphere: Nonylphenol Ethoxylate Degradation under UV and Solar Irradiation. *J. Alloys Compd.* **2016**, *678*, 126–136. [[CrossRef](#)]
10. Kashid, S.B.; Raut, R.W.; Malghe, Y.S. Microwave Assisted Synthesis of Nickel Nanostructures by Hydrazine Reduction Route: Effect of Solvent and Capping Agent on Morphology and Magnetic Properties. *Mater. Chem. Phys.* **2016**, *170*, 24–31. [[CrossRef](#)]
11. Kisukuri, C.M.; Palmeira, D.J.; Rodrigues, T.S.; Camargo, P.H.C.; Andrade, L.H. Bimetallic Nanoshells as Platforms for Metallo- and Biometallo-Catalytic Applications. *ChemCatChem* **2016**, *8*, 171–179. [[CrossRef](#)]
12. Da Silva, A.G.M.; Rodrigues, T.S.; Wang, J.; Yamada, L.K.; Alves, T.V.; Ornellas, F.R.; Ando, R.A.; Camargo, P.H.C. The Fault in Their Shapes: Investigating the Surface-Plasmon-Resonance-Mediated Catalytic Activities of Silver Quasi-Spheres, Cubes, Triangular Prisms, and Wires. *Langmuir* **2015**, *31*, 10272–10278. [[CrossRef](#)] [[PubMed](#)]
13. Da Silva, A.G.M.; Rodrigues, T.S.; Parussulo, A.L.A.; Candido, E.G.; Geonmonond, R.S.; Brito, H.F.; Toma, H.E.; Camargo, P.H.C. Controlled Synthesis of Nanomaterials at the Undergraduate Laboratory: Cu(OH)₂ and CuO Nanowires. *J. Chem. Educ.* **2017**, *94*, 743–750. [[CrossRef](#)]
14. Rodrigues, T.S.; da Silva, A.G.M.; de Oliveira, L.C.; da Silva, A.M.; Teixeira, R.R.; Camargo, P.H.C. Cu₂O Spheres as an Efficient Source of Catalytic Cu(I) Species for Performing Azide-Alkyne Click Reactions. *Tetrahedron Lett.* **2017**, *58*, 590–595. [[CrossRef](#)]
15. Estournés, C.; Lutz, T.; Happich, J.; Quaranta, T.; Wissler, P.; Guille, J.L. Nickel Nanoparticles in Silica Gel: Preparation and Magnetic Properties. *J. Magn. Magn. Mater.* **1997**, *173*, 83–92. [[CrossRef](#)]
16. Park, J.; Joo, J.; Kwon, S.G.; Jang, Y.; Hyeon, T. Synthesis of Monodisperse Spherical Nanocrystals. *Angew. Chem. Int. Ed.* **2007**, *46*, 4630–4660. [[CrossRef](#)]
17. You, H.; Fang, J. Particle-Mediated Nucleation and Growth of Solution-Synthesized Metal Nanocrystals: A New Story beyond the LaMer Curve. *Nano Today* **2016**, *11*, 145–167. [[CrossRef](#)]
18. LaMer, V.K.; Dinegar, R.H. Theory, Production and Mechanism of Formation of Monodispersed Hydrosols. *J. Am. Chem. Soc.* **1950**, *72*, 4847–4854. [[CrossRef](#)]
19. Jahangirian, H.; Kalantari, K.; Izadiyan, Z.; Rafiee-Moghaddam, R.; Shamel, K.; Webster, T.J. A Review of Small Molecules and Drug Delivery Applications Using Gold and Iron Nanoparticles. *Int. J. Nanomed.* **2019**, *14*, 1633–1657. [[CrossRef](#)]
20. Wang, H.; Jiao, X.; Chen, D. Monodispersed Nickel Nanoparticles with Tunable Phase and Size: Synthesis, Characterization, and Magnetic Properties. *J. Phys. Chem. C* **2008**, *112*, 18793–18797. [[CrossRef](#)]
21. Deepa, E.; Therese, H.A. Hierarchical Nickel Nanowire Synthesis Using Polysorbate 80 as Capping Agent. *Appl. Surf. Sci.* **2018**, *449*, 48–54. [[CrossRef](#)]
22. Başkaya, G.; Yıldız, Y.; Savk, A.; Okyay, T.O.; Eriş, S.; Sert, H.; Şen, F. Rapid, Sensitive, and Reusable Detection of Glucose by Highly Monodisperse Nickel Nanoparticles Decorated Functionalized Multi-Walled Carbon Nanotubes. *Biosens. Bioelectron.* **2017**, *91*, 728–733. [[CrossRef](#)]
23. Carenco, S.; Boissière, C.; Nicole, L.; Sanchez, C.; Le Floch, P.; Mézailles, N. Controlled Design of Size-Tunable Monodisperse Nickel Nanoparticles. *Chem. Mater.* **2010**, *22*, 1340–1349. [[CrossRef](#)]
24. Liu, X.; Liang, X.; Zhang, N.; Qiu, G.; Yi, R. Selective Synthesis and Characterization of Sea Urchin-like Metallic Nickel Nanocrystals. *Mater. Sci. Eng. B* **2006**, *132*, 272–277. [[CrossRef](#)]
25. Sidhaye, D.S.; Bala, T.; Srinath, S.; Srikanth, H.; Poddar, P.; Sastry, M.; Prasad, B.L.V. Preparation of Nearly Monodisperse Nickel Nanoparticles by a Facile Solution Based Methodology and Their Ordered Assemblies. *J. Phys. Chem. C* **2009**, *113*, 3426–3429. [[CrossRef](#)]
26. Wang, A.; Yin, H.; Lu, H.; Xue, J.; Ren, M.; Jiang, T. Catalytic Activity of Nickel Nanoparticles in Hydrogenation of P-Nitrophenol to p-Aminophenol. *Catal. Commun.* **2009**, *10*, 2060–2064. [[CrossRef](#)]
27. Mathew, A.; Munichandraiah, N.; Rao, G.M. Synthesis and Magnetic Studies of Flower-like Nickel Nanocones. *Mater. Sci. Eng. B* **2009**, *158*, 7–12. [[CrossRef](#)]
28. Wang, N.; Cao, X.; Kong, D.; Chen, W.; Guo, L.; Chen, C. Nickel Chains Assembled by Hollow Microspheres and Their Magnetic Properties. *J. Phys. Chem. C* **2008**, *112*, 6613–6619. [[CrossRef](#)]
29. Wang, D.-P.; Sun, D.-B.; Yu, H.-Y.; Meng, H.-M. Morphology Controllable Synthesis of Nickel Nanopowders by Chemical Reduction Process. *J. Cryst. Growth* **2008**, *310*, 1195–1201. [[CrossRef](#)]
30. Bao, J.; Liang, Y.; Xu, Z.; Si, L. Facile Synthesis of Hollow Nickel Submicrometer Spheres. *Adv. Mater.* **2003**, *15*, 1832–1835. [[CrossRef](#)]
31. Al Zoubi, W.; Putri, R.A.K.; Abukhadra, M.R.; Ko, Y.G. Recent Experimental and Theoretical Advances in the Design and Science of High-Entropy Alloy Nanoparticles. *Nano Energy* **2023**, *110*, 108362. [[CrossRef](#)]
32. Guan, J.; Liu, L.; Xu, L.; Sun, Z.; Zhang, Y. Nickel Flower-like Nanostructures Composed of Nanoplates: One-Pot Synthesis, Stepwise Growth Mechanism and Enhanced Ferromagnetic Properties. *CrystEngComm* **2011**, *13*, 2636. [[CrossRef](#)]
33. Tang, S.; Vongehr, S.; Ren, H.; Meng, X. Diameter-Controlled Synthesis of Polycrystalline Nickel Nanowires and Their Size Dependent Magnetic Properties. *CrystEngComm* **2012**, *14*, 7209. [[CrossRef](#)]
34. Wang, H.; Kou, X.; Zhang, L.; Li, J. Size-Controlled Synthesis, Microstructure and Magnetic Properties of Ni Nanoparticles. *Mater. Res. Bull.* **2008**, *43*, 3529–3536. [[CrossRef](#)]
35. Khanna, P.K.; More, P.V.; Jawalkar, J.P.; Bharate, B.G. Effect of Reducing Agent on the Synthesis of Nickel Nanoparticles. *Mater. Lett.* **2009**, *63*, 1384–1386. [[CrossRef](#)]

36. Chandra, S.; Kumar, A.; Tomar, P.K. Synthesis of Ni Nanoparticles and Their Characterizations. *J. Saudi Chem. Soc.* **2014**, *18*, 437–442. [[CrossRef](#)]
37. Eluri, R.; Paul, B. Microwave Assisted Greener Synthesis of Nickel Nanoparticles Using Sodium Hypophosphite. *Mater. Lett.* **2012**, *76*, 36–39. [[CrossRef](#)]
38. Soumare, Y.; Dakhlaoui-Omrani, A.; Schoenstein, F.; Mercone, S.; Viau, G.; Jouini, N. Nickel Nanofibers and Nanowires: Elaboration by Reduction in Polyol Medium Assisted by External Magnetic Field. *Solid. State Commun.* **2011**, *151*, 284–288. [[CrossRef](#)]
39. Metin, Ö.; Mazumder, V.; Özkar, S.; Sun, S. Monodisperse Nickel Nanoparticles and Their Catalysis in Hydrolytic Dehydrogenation of Ammonia Borane. *J. Am. Chem. Soc.* **2010**, *132*, 1468–1469. [[CrossRef](#)] [[PubMed](#)]
40. Jeon, Y.T.; Moon, J.Y.; Lee, G.H.; Park, J.; Chang, Y. Comparison of the Magnetic Properties of Metastable Hexagonal Close-Packed Ni Nanoparticles with Those of the Stable Face-Centered Cubic Ni Nanoparticles. *J. Phys. Chem. B* **2006**, *110*, 1187–1191. [[CrossRef](#)]
41. Railsback, J.G.; Johnston-Peck, A.C.; Wang, J.; Tracy, J.B. Size-Dependent Nanoscale Kirkendall Effect During the Oxidation of Nickel Nanoparticles. *ACS Nano* **2010**, *4*, 1913–1920. [[CrossRef](#)]
42. Chen, D.-H.; Hsieh, C.-H. Synthesis of Nickel Nanoparticles in Aqueous Cationic Surfactant Solutions. *J. Mater. Chem.* **2002**, *12*, 2412–2415. [[CrossRef](#)]
43. Huang, G.; Xu, S.; Xu, G.; Li, L.; Zhang, L. Preparation of Fine Nickel Powders via Reduction of Nickel Hydrazine Complex Precursors. *Trans. Nonferrous Met. Soc. China* **2009**, *19*, 389–393. [[CrossRef](#)]
44. Duan, X.; Qian, G.; Liu, Y.; Ji, J.; Zhou, X.; Chen, D.; Yuan, W. Structure Sensitivity of Ammonia Decomposition over Ni Catalysts: A Computational and Experimental Study. *Fuel Process. Technol.* **2013**, *108*, 112–117. [[CrossRef](#)]
45. Park, J.W.; Chae, E.H.; Kim, S.H.; Lee, J.H.; Kim, J.W.; Yoon, S.M.; Choi, J.J.-Y. Preparation of Fine Ni Powders from Nickel Hydrazine Complex. *Mater. Chem. Phys.* **2006**, *97*, 371–378. [[CrossRef](#)]
46. Guo, L.; Liu, C.; Wang, R.; Xu, H.; Wu, Z.; Yang, S. Large-Scale Synthesis of Uniform Nanotubes of a Nickel Complex by a Solution Chemical Route. *J. Am. Chem. Soc.* **2004**, *126*, 4530–4531. [[CrossRef](#)]
47. Gao, C.; Lu, Z.; Yin, Y. Gram-Scale Synthesis of Silica Nanotubes with Controlled Aspect Ratios by Templating of Nickel-Hydrazine Complex Nanorods. *Langmuir* **2011**, *27*, 12201–12208. [[CrossRef](#)] [[PubMed](#)]
48. Nelson, N.C.; Ruberu, T.P.A.; Reichert, M.D.; Vela, J. Templated Synthesis and Chemical Behavior of Nickel Nanoparticles within High Aspect Ratio Silica Capsules. *J. Phys. Chem. C* **2013**, *117*, 25826–25836. [[CrossRef](#)]
49. Zhou, S.; Yang, T.-H.; Zhao, M.; Xia, Y. Quantitative Analysis of the Reduction Kinetics of a Pt(II) Precursor in the Context of Pt Nanocrystal Synthesis. *Chin. J. Chem. Phys.* **2018**, *31*, 370–374. [[CrossRef](#)]
50. Rodrigues, T.S.; Zhao, M.; Yang, T.; Gilroy, K.D.; da Silva, A.G.M.; Camargo, P.H.C.; Xia, Y. Synthesis of Colloidal Metal Nanocrystals: A Comprehensive Review on the Reductants. *Chem. A Eur. J.* **2018**, *24*, 16944–16963. [[CrossRef](#)]
51. Carroll, K.J.; Reveles, J.U.; Shultz, M.D.; Khanna, S.N.; Carpenter, E.E. Preparation of Elemental Cu and Ni Nanoparticles by the Polyol Method: An Experimental and Theoretical Approach. *J. Phys. Chem. C* **2011**, *115*, 2656–2664. [[CrossRef](#)]
52. Song, H.-J.; Jia, X.-H.; Yang, X.-F.; Tang, H.; Li, Y.; Su, Y.-T. Controllable Synthesis of Monodisperse Polyhedral Nickelnanocrystals. *CrystEngComm* **2012**, *14*, 405–410. [[CrossRef](#)]
53. Skrabalak, S.E.; Wiley, B.J.; Kim, M.; Formo, E.V.; Xia, Y. On the Polyol Synthesis of Silver Nanostructures: Glycolaldehyde as a Reducing Agent. *Nano Lett.* **2008**, *8*, 2077–2081. [[CrossRef](#)]
54. Fievet, F.; Lagier, J.P.; Figlarz, M. Preparing Monodisperse Metal Powders in Micrometer and Submicrometer Sizes by the Polyol Process. *MRS Bull.* **1989**, *14*, 29–34. [[CrossRef](#)]
55. Ying, Z.; Shengming, J.; Guanzhou, Q.; Min, Y. Preparation of Ultrafine Nickel Powder by Polyol Method and Its Oxidation Product. *Mater. Sci. Eng. B* **2005**, *122*, 222–225. [[CrossRef](#)]
56. Couto, G.G.; Klein, J.J.; Schreiner, W.H.; Mosca, D.H.; de Oliveira, A.J.A.; Zarbin, A.J.G. Nickel Nanoparticles Obtained by a Modified Polyol Process: Synthesis, Characterization, and Magnetic Properties. *J. Colloid. Interface Sci.* **2007**, *311*, 461–468. [[CrossRef](#)] [[PubMed](#)]
57. Roselina, N.R.N.; Azizan, A. Ni Nanoparticles: Study of Particles Formation and Agglomeration. *Procedia Eng.* **2012**, *41*, 1620–1626. [[CrossRef](#)]
58. Wu, S.-H.; Chen, D.-H. Synthesis and Characterization of Nickel Nanoparticles by Hydrazine Reduction in Ethylene Glycol. *J. Colloid. Interface Sci.* **2003**, *259*, 282–286. [[CrossRef](#)] [[PubMed](#)]
59. Liu, C.-M.; Guo, L.; Wang, R.-M.; Deng, Y.; Xu, H.-B.; Yang, S. Magnetic Nanochains of Metal Formed by Assembly of Small Nanoparticles. *Chem. Commun.* **2004**, 2726. [[CrossRef](#)] [[PubMed](#)]
60. Zhou, W.; Guo, L.; He, L.; Chen, C.P. Synthesis, Characterization, and Magnetic Properties of Flower-like Nickel Materials. *Phys. Status Solidi (A)* **2008**, *205*, 1109–1112. [[CrossRef](#)]
61. Tzitzios, V.; Basina, G.; Gjoka, M.; Alexandrakis, V.; Georgakilas, V.; Niarchos, D.; Boukos, N.; Petridis, D. Chemical Synthesis and Characterization of Hcp Ni Nanoparticles. *Nanotechnology* **2006**, *17*, 3750–3755. [[CrossRef](#)]
62. Hu, X.; Yu, J.C. High-Yield Synthesis of Nickel and Nickel Phosphide Nanowires via Microwave-Assisted Processes. *Chem. Mater.* **2008**, *20*, 6743–6749. [[CrossRef](#)]
63. Biacchi, A.J.; Schaak, R.E. The Solvent Matters: Kinetic versus Thermodynamic Shape Control in the Polyol Synthesis of Rhodium Nanoparticles. *ACS Nano* **2011**, *5*, 8089–8099. [[CrossRef](#)]

64. Wang, Y.; Peng, H.-C.; Liu, J.; Huang, C.Z.; Xia, Y. Use of Reduction Rate as a Quantitative Knob for Controlling the Twin Structure and Shape of Palladium Nanocrystals. *Nano Lett.* **2015**, *15*, 1445–1450. [[CrossRef](#)]
65. Niu, W.; Li, Z.-Y.; Shi, L.; Liu, X.; Li, H.; Han, S.; Chen, J.; Xu, G. Seed-Mediated Growth of Nearly Monodisperse Palladium Nanocubes with Controllable Sizes. *Cryst. Growth Des.* **2008**, *8*, 4440–4444. [[CrossRef](#)]
66. O'Brien, W.L.; Tonner, B.P. Transition to the Perpendicular Easy Axis of Magnetization in Ni Ultrathin Films Found by X-ray Magnetic Circular Dichroism. *Phys. Rev. B* **1994**, *49*, 15370–15373. [[CrossRef](#)] [[PubMed](#)]
67. Niu, H.; Chen, Q.; Zhu, H.; Lin, Y.; Zhang, X. Magnetic Field-Induced Growth and Self-Assembly of Cobalt Nanocrystallites. *J. Mater. Chem.* **2003**, *13*, 1803. [[CrossRef](#)]
68. Yang, H.G.; Zeng, H.C. Preparation of Hollow Anatase TiO₂ Nanospheres via Ostwald Ripening. *J. Phys. Chem. B* **2004**, *108*, 3492–3495. [[CrossRef](#)] [[PubMed](#)]
69. Hu, H.; Sugawara, K. Magnetic-Field-Assisted Synthesis of Ni Nanostructures: Selective Control of Particle Shape. *Chem. Phys. Lett.* **2009**, *477*, 184–188. [[CrossRef](#)]
70. Heidari, N.; Ghiasvand, A. A Review on Magnetic Field-Assisted Solid-Phase Microextraction Techniques. *J. Liq. Chromatogr. Relat. Technol.* **2020**, *43*, 75–82. [[CrossRef](#)]
71. Zhang, J.; Xiang, W.; Liu, Y.; Hu, M.; Zhao, K. Synthesis of High-Aspect-Ratio Nickel Nanowires by Dropping Method. *Nanoscale Res. Lett.* **2016**, *11*, 118. [[CrossRef](#)]
72. Ni, X.; Zhao, Q.; Zhang, D.; Zhang, X.; Zheng, H. Novel Hierarchical Nanostructures of Nickel: Self-Assembly of Hexagonal Nanoplatelets. *J. Phys. Chem. C* **2007**, *111*, 601–605. [[CrossRef](#)]
73. Shevchenko, E.V.; Talapin, D.V.; Schnablegger, H.; Kornowski, A.; Festin, Ö.; Svedlindh, P.; Haase, M.; Weller, H. Study of Nucleation and Growth in the Organometallic Synthesis of Magnetic Alloy Nanocrystals: The Role of Nucleation Rate in Size Control of CoPt₃ Nanocrystals. *J. Am. Chem. Soc.* **2003**, *125*, 9090–9101. [[CrossRef](#)]
74. Omrani, A.D.; Bousnina, M.A.; Smiri, L.S.; Taibi, M.; Leone, P.; Schoenstein, F.; Jouini, N. Elaboration of Nickel Nanoparticles by Modified Polyol Process and Their Spark Plasma Sintering, Characterization and Magnetic Properties of the Nanoparticles and the Dense Nano-Structured Material. *Mater. Chem. Phys.* **2010**, *123*, 821–828. [[CrossRef](#)]
75. Ni, Y.; Tao, A.; Hu, G.; Cao, X.; Wei, X.; Yang, Z. Synthesis, Characterization and Properties of Hollow Nickel Phosphide Nanospheres. *Nanotechnology* **2006**, *17*, 5013–5018. [[CrossRef](#)]
76. Liu, Q.; Liu, H.; Han, M.; Zhu, J.; Liang, Y.; Xu, Z.; Song, Y. Nanometer-Sized Nickel Hollow Spheres. *Adv. Mater.* **2005**, *17*, 1995–1999. [[CrossRef](#)]
77. Yu, L.; Banerjee, I.A.; Shima, M.; Rajan, K.; Matsui, H. Size-Controlled Ni Nanocrystal Growth on Peptide Nanotubes and Their Magnetic Properties. *Adv. Mater.* **2004**, *16*, 709–712. [[CrossRef](#)]
78. Abedini, A.; Daud, A.R.; Hamid, M.A.A.; Othman, N.K.; Saion, E. A Review on Radiation-Induced Nucleation and Growth of Colloidal Metallic Nanoparticles. *Nanoscale Res. Lett.* **2013**, *8*, 474. [[CrossRef](#)]
79. Alex, S.; Tiwari, A. Functionalized Gold Nanoparticles: Synthesis, Properties and Applications—A Review. *J. Nanosci. Nanotechnol.* **2015**, *15*, 1869–1894. [[CrossRef](#)] [[PubMed](#)]
80. Hou, Y.; Kondoh, H.; Ohta, T.; Gao, S. Size-Controlled Synthesis of Nickel Nanoparticles. *Appl. Surf. Sci.* **2005**, *241*, 218–222. [[CrossRef](#)]
81. Salim, M.; Minamikawa, H.; Sugimura, A.; Hashim, R. Amphiphilic Designer Nano-Carriers for Controlled Release: From Drug Delivery to Diagnostics. *Med. Chem. Commun.* **2014**, *5*, 1602–1618. [[CrossRef](#)]
82. Singla, M.L.; Negi, A.; Mahajan, V.; Singh, K.C.; Jain, D.V.S. Catalytic Behavior of Nickel Nanoparticles Stabilized by Lower Alkylammonium Bromide in Aqueous Medium. *Appl. Catal. A Gen.* **2007**, *323*, 51–57. [[CrossRef](#)]
83. Huang, G.; Xu, S.; Li, L.; Wang, X. Effect of Surfactants on Dispersion Property and Morphology of Nano-Sized Nickel Powders. *Trans. Nonferrous Met. Soc. China* **2014**, *24*, 3739–3746. [[CrossRef](#)]
84. Wang, A.; Yin, H.; Lu, H.; Xue, J.; Ren, M.; Jiang, T. Effect of Organic Modifiers on the Structure of Nickel Nanoparticles and Catalytic Activity in the Hydrogenation of *p*-Nitrophenol to *p*-Aminophenol. *Langmuir* **2009**, *25*, 12736–12741. [[CrossRef](#)]
85. Ramírez-Meneses, E.; Torres-Huerta, A.M.; Domínguez-Crespo, M.A.; Ponce-Varela, M.G.; Hernández-Pérez, M.A.; Betancourt, I.; Palacios-González, E. Synthesis and Electrochemical Characterization of Ni Nanoparticles by Hydrazine Reduction Using Hydroxyethyl Cellulose as Capping Agent. *Electrochim. Acta* **2014**, *127*, 228–238. [[CrossRef](#)]
86. Ni, X.; Zhao, Q.; Zhang, D.; Yang, D.; Zheng, H. Large Scaled Synthesis of Chainlike Nickel Wires Assisted by Ligands. *J. Cryst. Growth* **2005**, *280*, 217–221. [[CrossRef](#)]
87. Singh, K.; Kate, K.H.; Chilukuri, V.V.S.; Khanna, P.K. Glycerol Mediated Low Temperature Synthesis of Nickel Nanoparticles by Solution Reduction Method. *J. Nanosci. Nanotechnol.* **2011**, *11*, 5131–5136. [[CrossRef](#)]
88. Zhang, J.; Ohara, S.; Umetsu, M.; Naka, T.; Hatakeyama, Y.; Adschiri, T. Colloidal Ceria Nanocrystals: A Tailor-Made Crystal Morphology in Supercritical Water. *Adv. Mater.* **2007**, *19*, 203–206. [[CrossRef](#)]
89. Huang, Y.Y.; Zhou, Y.C.; Pan, Y. Effects of Hydrogen Adsorption on the Surface-Energy Anisotropy of Nickel. *Phys. B Condens. Matter.* **2010**, *405*, 1335–1338. [[CrossRef](#)]
90. Leng, Y.; Li, Y.; Li, X.; Takahashi, S. Improved Magnetic Anisotropy of Monodispersed Triangular Nickel Nanoplates. *J. Phys. Chem. C* **2007**, *111*, 6630–6633. [[CrossRef](#)]
91. Blakely, J.M.; Mykura, H. The Effect of Impurity Adsorption on the Surface Energy and Surface Self Diffusion in Nickel. *Acta Metall.* **1961**, *9*, 595–599. [[CrossRef](#)]

92. Fu, Y.; Pichon, B.; Devred, F.; Singleton, M.L.; Hermans, S. Synthesis of Spherical, Rod, or Chain Ni Nanoparticles and Their Structure–Activity Relationship in Glucose Hydrogenation Reaction. *J. Catal.* **2022**, *415*, 63–76. [[CrossRef](#)]
93. Cho, H.; Lee, N.; Kim, B.H. Synthesis of Highly Monodisperse Nickel and Nickel Phosphide Nanoparticles. *Nanomaterials* **2022**, *12*, 3198. [[CrossRef](#)]
94. He, M.; Ai, Y.; Hu, W.; Guan, L.; Ding, M.; Liang, Q. Recent Advances of Seed-Mediated Growth of Metal Nanoparticles: From Growth to Applications. *Adv. Mater.* **2023**, *35*, 2211915. [[CrossRef](#)]
95. Jiang, Y.; Tao, R.; Zhang, H.; Wan, N.; Yang, Y.; Gu, D.; Zhang, T.; Rui, Y.; Xu, J. Separating Nucleation from Growth for High-Yield Synthesis of Thin Silver Nanowires. *J. Mater. Sci. Mater. Electron.* **2023**, *34*, 26. [[CrossRef](#)]
96. Kuchkina, N.; Sorokina, S.; Torozova, A.; Bykov, A.; Shifrina, Z. Ni Nanoparticles Entrapped by a Functional Dendrimer as a Highly Efficient and Recyclable Catalyst for Suzuki-Miyaura Cross-Coupling Reactions. *ChemistrySelect* **2022**, *7*, e202202653. [[CrossRef](#)]
97. Moreira, M.; Felix, L.C.; Cottancin, E.; Pellarin, M.; Ugarte, D.; Hillenkamp, M.; Galvao, D.S.; Rodrigues, V. Influence of Cluster Sources on the Growth Mechanisms and Chemical Composition of Bimetallic Nanoparticles. *J. Phys. Chem. C* **2023**, *127*, 1944–1954. [[CrossRef](#)]
98. Bai, L.; Yuan, F.; Tang, Q. Synthesis of Nickel Nanoparticles with Uniform Size via a Modified Hydrazine Reduction Route. *Mater. Lett.* **2008**, *62*, 2267–2270. [[CrossRef](#)]
99. Liu, S.; Li, Z.; Yu, B.; Wang, S.; Shen, Y.; Cong, H. Recent Advances on Protein Separation and Purification Methods. *Adv. Colloid. Interface Sci.* **2020**, *284*, 102254. [[CrossRef](#)]
100. Robertson, J.D.; Rizzello, L.; Avila-Olias, M.; Gaitzsch, J.; Contini, C.; Magoń, M.S.; Renshaw, S.A.; Battaglia, G. Purification of Nanoparticles by Size and Shape. *Sci. Rep.* **2016**, *6*, 27494. [[CrossRef](#)]
101. Rodrigues, T.S.; e Silva, F.A.; Candido, E.G.; da Silva, A.G.M.; dos Geonmonond, R.S.; Camargo, P.H.C.; Linardi, M.; Fonseca, F.C. Ethanol Steam Reforming: Understanding Changes in the Activity and Stability of Rh/MxOy Catalysts as Function of the Support. *J. Mater. Sci.* **2019**, *54*, 11400–11416. [[CrossRef](#)]
102. Stephens, J.R.; Beveridge, J.S.; Williams, M.E. Analytical Methods for Separating and Isolating Magnetic Nanoparticles. *Phys. Chem. Chem. Phys.* **2012**, *14*, 3280. [[CrossRef](#)] [[PubMed](#)]
103. Bouremana, A.; Mouaci, S.; Berriah, A.; Boutebina, Z.; Manseri, A.; Bensouilah, A. High Yield Solvothermal Synthesis of Ni Nanoparticles: Structural, Microstructural, and Magnetic Properties. *J. Nanopart. Res.* **2022**, *24*, 204. [[CrossRef](#)]
104. Le, T.-D.; Suttikhana, I.; Ashaolu, T.J. State of the Art on the Separation and Purification of Proteins by Magnetic Nanoparticles. *J. Nanobiotechnology* **2023**, *21*, 363. [[CrossRef](#)]
105. Ikeda, K.; Shimoyama, Y.; Orita, Y. Efficient Purification of Surface Modified Nanoparticles from Its Nanosuspension by Using Supercritical CO₂ Technology. *J. Supercrit. Fluids* **2023**, *199*, 105966. [[CrossRef](#)]
106. Mouaci, S.; Bouremana, A.; Boutebina, Z.; Berriah, A.; Manseri, A.; Saidi, M.; Saidi-Amroun, N. Enhancing LDPE Performance Using Ni Nanoparticles: A Comprehensive Study of Structural, Magnetic, and Mechanical Properties. *J. Polym. Res.* **2023**, *30*, 374. [[CrossRef](#)]

Disclaimer/Publisher’s Note: The statements, opinions and data contained in all publications are solely those of the individual author(s) and contributor(s) and not of MDPI and/or the editor(s). MDPI and/or the editor(s) disclaim responsibility for any injury to people or property resulting from any ideas, methods, instructions or products referred to in the content.